

**DYNAMIC SIMULATIONS OF NOVEL OLIGOMERS CONTAINING  
FLUORINATED SEGMENTS**

by

**ÜNAL ŞEN**

**B.S. in Chem., Bilkent University, 2002**

**Submitted to the Graduate School of Engineering and Natural Sciences**

**in partial fulfillment of**

**the requirements for the degree of**

**Master of Science**

**Sabancı University**

**Spring 2004**



© Ünal Şen 2004

All Rights Reserved

## ABSTRACT

Nowadays, many fluorinated polymers are designed for novel applications. Computational studies are very important in understanding their properties from a theoretical point of view. In this thesis, we carry out computer simulations of linear and graft fluorinated polymers at the quantum level as well as the atomistic and mesoscopic scales. The semiempirical quantum mechanical approach can not optimize the structure of the polymers to their global minima of the potential energy surface and is not an appropriate method for conformational search analysis of the long chain polymers. On the other hand, it can be used to predict  $^{13}\text{C}$  chemical shifts and heats of formation. We performed MD simulations on bulk linear fluorinated polymers under external electric field to investigate the effects of strong electric field on the conformational properties of the polymers. Cyanide functional groups in the polymer are aligned along the applied electric field due to their polarity. A total alignment of the cyanide groups is observed only at electric fields on the order of  $10^{11}$  V/m. We observe that polarization increases with increased electric field and density of the system. We also used two mesoscale simulation methods, Dissipative Particle Dynamics (DPD) and MesoDyn, to simulate the polymer-solvent mesophase morphologies of the graft and fluorinated polymers at different concentrations. It is observed that both polymers have spherical morphology in an aprotic solvent. Although DPD and MesoDyn use different approaches for the simulation of mesoscale structures, they give similar results and can be used interchangeably to predict three-dimensional phase behaviour. We predict that the wettability of the linear polymers should be higher than that of the graft, and this is in accordance with experimental findings on these systems.

## ÖZET

Günümüzde yeni uygulamaları olan birçok florlu polimer tasarlanmaktadır. Bu polimerlerin özelliklerini teorik açıdan anlamak için hesaplamasal çalışmalar önemli bir yer teşkil etmektedir. Bu tezde, düzgün ve graft polimerlere kuvantum, atomic ve mezo ölçeklerde bilgisayar simülasyonları yapıldı. Yarı deneysel kuvantum metodu polimerlerin yapısını potansiyel enerji yüzeyindeki global minimum seviyesine kadar optimize etmede başarısız bulunmuştur ve bu metod uzun zincirli polimerlerin konformasyonel araştırma analizleri için uygun değildir. Öbür taraftan yarı deneysel kuvantum metodları  $^{13}\text{C}$  kimyasal kaymaları ve oluşma enerjilerini tahmin etmede kullanılabilir. Güçlü elektrik alanının polimerlerin konformasyonel özellikleri üzerindeki etkilerini anlamak için bulk florlu polimer sistemlerine elektrik alanında MD simülasyonları yapıldı.  $-\text{CN}$  fonksiyonel gruplarının polar özelliğinden dolayı elektrik alan doğrultusunda yöneltiler ve tam yönelim  $10^{11}$  V/m mertebesinde gerçekleşti. Polarizasyonun sistemin özkütlesi ve uygulanan elektrik alanla arttığını gözlemledik. Graft ve düzgün polimerlerin değişik oranlardaki polimer-çözücü faz morfolojilerini anlamak için mezo ölçekli simülasyon metodları kullanıldı (Dissipative Particle Dynamics ve Mesodyn). Çözücü içerisinde iki polimer de küresel morfolojilere sahip olduğu gözlemlendi. İki metod mezo ölçekte simülasyonlar için farklı yaklaşımlar kullanmasına rağmen benzer sonuçlar verdi ve birbirlerinin yerine kullanılabilirler.

## ACKNOWLEDGEMENTS

It is great pleasure to thank my supervisor Canan Baysal for introducing me this interesting and exciting area of research, and for her endless encouragement and guidance during this study. I greatly appreciate the influence she has had on my personal development as a researcher.

I would like to express my thanks to Yusuf Mencelođlu and Rahmi Özışık for serving on my graduate committee and for devoting their valuable time to reading and commenting on the thesis.

I also want to thank my friends Hüsnü Ada, Serkan Baş, Burak Birkan, Özgür Bozat, Karahan Bulut, Mustafa Çoban, Alisher Kholmatov, Mehmet Özdemir, Güngör Özer, Mustafa Parlak, Yener Kuru, Mesut Ünal and all my friends at Sabancı University. They were always near me and motivated me to study harder on my thesis.

Finally, I would like to express my grateful thanks to my parents, sisters, brothers, sweet nieces and nephews.

## TABLE OF CONTENTS

ABSTRACT .....	iv
ÖZET .....	v
ACKNOWLEDGMENT .....	vi
LIST OF TABLES .....	ix
LIST OF FIGURES .....	x
LIST OF SYMBOLS .....	xi
LIST OF ABBREVIATIONS .....	xii
1. INTRODUCTION .....	1
2. ATOMISTIC SIMULATIONS OF SINGLE CHAIN AND BULK FLUORINATED POLYMERS .....	6
2.1. Molecular Model and Computational Methods .....	6
2.1.1. Molecular Dynamics .....	6
2.1.2. Minimization Methods .....	8
2.1.3. Semiempirical Approaches .....	9
2.2. Results And Discussion .....	12
2.2.1. Semiempirical Calculations .....	12
2.2.2. Molecular Dynamics Simulations of Bulk Systems of Fluorinated Polymers Under External Electric Field .....	17
3. MESOSCOPIC MORPHOLOGIES OF FLUORINATED OLIGOMERS IN AN APROTIC SOLVENT .....	23
3.1. Molecular Model and Computational Methods .....	23
3.1.1. Dissipative Particle Dynamics .....	24
3.1.2. Mesodyn .....	27

3.2. Results and Discussion .....	30
3.2.1. Interaction Energies and Parameterization .....	30
3.2.2. Mesoscale Calculations of The Fluorinated Polymers .....	35
3.2.2.1.Dissipative Particle Dynamics Simulations .....	35
3.2.2.2.Mesodyn Simulations .....	41
4. CONCLUSIONS AND SUGGESTIONS FOR FUTURE WORK .....	43
APPENDIX A: CONSISTENT FORCEFIELD-COMPASS .....	46
BIBLIOGRAPHY .....	48

## LIST OF TABLES

Table 3.1.	Beads used in the DPD and MesoDyn simulations .....	31
Table 3.2.	Solubility parameters and molar volumes of the beads .....	32
Table 3.3.	Flory-Huggins, conservative repulsion, and MesoDyn parameters .....	34
Table 3.4.	Interfacial tensions at different concentrations .....	40

## LIST OF FIGURES

Figure 2.1.	Evaluation of heats of formation of linear fluorinated polymer (a) long polymer chain and, (b) small polymer chain .....	13
Figure 2.2.	Predicted NMR shifts of (a) long and, (b) short chains .....	16
Figure 2.3.	Polarization vs. Electric field .....	18
Figure 2.4.	Views on the xy-plane of LFP40 system. Initial configuration before starting external electric field in the (a) +z direction and (b)-z direction; after applying electric field for 600 ps (c) +z direction and (d) -z direction .....	19
Figure 2.5.	Views on the xy-plane of LFP10 system. Initial configuration before starting external electric field in the (a)-z direction; after applying electric field for 600 ps (b) -z direction .....	20
Figure 2.6.	Views on the xy-plane of LFP20 system. Initial configuration external electric field in the (a)-z direction; after applying electric field for 600 ps (b) -z direction .....	21
Figure 3.1.	(a) Linear fluorinated polymer (b) Graft fluorinated polymer .....	24
Figure 3.2.	Radial distribution function .....	36
Figure 3.3.	Isosurface morphologies of linear fluorinated polymers at different concentrations (a) 20% in DMF (b) 30% in DMF (c) 40% in DMF (d) pure polymer .....	37
Figure 3.4.	Isosurface morphologies of graft fluorinated polymers at different concentrations (a) 20% in DMF (b) 30% in DMF (c) 40% in DMF (d) pure polymer .....	38
Figure 3.5.	RMS end-to-end distances of linear and graft fluorinated polymers .....	39
Figure 3.6.	Isosurface representations of the (a) Pure linear polymer (b) 20% Graft polymer .....	41

## LIST OF SYMBOLS

$\text{\AA}$	Angstrom
$k$	Boltzmann constant
$\epsilon_s$	Static dielectric constant
$E$	Energy of the system
$\chi_{AB}$	Flory-Huggins parameter
$N$	Number of atoms
$P$	Pressure
$\delta$	Solubility parameter
$T$	Temperature
$V_{bead}$	Molar volume of a bead
$\Psi$	Molecular orbital wave function

## LIST OF ABBREVIATIONS

AM1	Austin Model 1
AO	Atomic Orbital
CG	Conjugate Gradient
CI	Configuration Interaction
COMPASS	Condensed-phase Optimized Molecular Potentials for Atomistic Simulation Studies
DPD	Dissipative Particle Dynamics
FH	Flory-Huggins
HE	Half-Electron
GFP	Graft Fluorinated Polymer
LCAO	Linear Combination of Atomic Orbitals
LCAO-SCF	Linear Combination of Atomic Orbitals-Self Consistent Field
LFP	Linear Fluorinated Polymer
MC	Monte Carlo
MD	Molecular Dynamics
MNDO	Modified Neglect of Diatomic Overlap
MO	Molecular Orbital
PM3	Parametric Method Number 3
SCF	Self-Consistent Field
RDF	Radial Distribution Function
RHF	Restricted Hartree-Fock
RMS	Root Mean Square
SD	Steepest Descent

**DYNAMIC SIMULATIONS OF NOVEL OLIGOMERS CONTAINING  
FLUORINATED SEGMENTS**

by

**ÜNAL ŞEN**

**B.S. in Chem., Bilkent University, 2002**

**Submitted to the Graduate School of Engineering and Natural Sciences**

**in partial fulfillment of**

**the requirements for the degree of**

**Master of Science**

**Sabancı University**

**Spring 2004**



© Ünal Şen 2004

All Rights Reserved

## ABSTRACT

Nowadays, many fluorinated polymers are designed for novel applications. Computational studies are very important in understanding their properties from a theoretical point of view. In this thesis, we carry out computer simulations of linear and graft fluorinated polymers at the quantum level as well as the atomistic and mesoscopic scales. The semiempirical quantum mechanical approach can not optimize the structure of the polymers to their global minima of the potential energy surface and is not an appropriate method for conformational search analysis of the long chain polymers. On the other hand, it can be used to predict  $^{13}\text{C}$  chemical shifts and heats of formation. We performed MD simulations on bulk linear fluorinated polymers under external electric field to investigate the effects of strong electric field on the conformational properties of the polymers. Cyanide functional groups in the polymer are aligned along the applied electric field due to their polarity. A total alignment of the cyanide groups is observed only at electric fields on the order of  $10^{11}$  V/m. We observe that polarization increases with increased electric field and density of the system. We also used two mesoscale simulation methods, Dissipative Particle Dynamics (DPD) and MesoDyn, to simulate the polymer-solvent mesophase morphologies of the graft and fluorinated polymers at different concentrations. It is observed that both polymers have spherical morphology in an aprotic solvent. Although DPD and MesoDyn use different approaches for the simulation of mesoscale structures, they give similar results and can be used interchangeably to predict three-dimensional phase behaviour. We predict that the wettability of the linear polymers should be higher than that of the graft, and this is in accordance with experimental findings on these systems.

## ÖZET

Günümüzde yeni uygulamaları olan birçok florlu polimer tasarlanmaktadır. Bu polimerlerin özelliklerini teorik açıdan anlamak için hesaplamasal çalışmalar önemli bir yer teşkil etmektedir. Bu tezde, düzgün ve graft polimerlere kuvantum, atomic ve mezo ölçeklerde bilgisayar simülasyonları yapıldı. Yarı deneysel kuvantum metodu polimerlerin yapısını potansiyel enerji yüzeyindeki global minimum seviyesine kadar optimize etmede başarısız bulunmuştur ve bu metod uzun zincirli polimerlerin konformasyonel araştırma analizleri için uygun değildir. Öbür taraftan yarı deneysel kuvantum metodları <sup>13</sup>C kimyasal kaymaları ve oluşma enatlpilerini tahmin etmede kullanılabilir. Güçlü elektrik alanının polimerlerin konformasyonel özellikleri üzerindeki etkilerini anlamak için bulk florlu polimer sistemlerine elektrik alanda MD simülasyonları yapıldı. -CN fonksiyonel gruplarının polar özelliğinden dolayı elektrik alan doğrultusunda yöneldiler ve tam yönelim 10<sup>11</sup> V/m mertebesinde gerçekleşti. Polarizasyonun sistemin özkütlesi ve uygulanan elektrik alanla arttığını gözlemledik. Graft ve düzgün polimerlerin değişik oranlardaki polimer-çözücü faz morfolojilerini anlamak için mezo ölçekli simülasyon metodları kullanıldı (Dissipative Particle Dynamics ve Mesodyn). Çözücü içerisinde iki polimer de küresel morfolojilere sahip olduğu gözlemlendi. İki metod mezo ölçekte simülasyonlar için farklı yaklaşımlar kullanmasına rağmen benzer sonuçlar verdi ve birbirlerinin yerine kullanılabilirler.

## ACKNOWLEDGEMENTS

It is great pleasure to thank my supervisor Canan Baysal for introducing me this interesting and exciting area of research, and for her endless encouragement and guidance during this study. I greatly appreciate the influence she has had on my personal development as a researcher.

I would like to express my thanks to Yusuf Mencilođlu and Rahmi Özişik for serving on my graduate committee and for devoting their valuable time to reading and commenting on the thesis.

I also want to thank my friends Hüsnü Ada, Serkan Baş, Burak Birkan, Özgür Bozat, Karahan Bulut, Mustafa Çoban, Alisher Kholmatov, Mehmet Özdemir, Güngör Özer, Mustafa Parlak, Yener Kuru, Mesut Ünal and all my friends at Sabancı University. They were always near me and motivated me to study harder on my thesis.

Finally, I would like to express my grateful thanks to my parents, sisters, brothers, sweet nieces and nephews.

## TABLE OF CONTENTS

ABSTRACT .....	iv
ÖZET .....	v
ACKNOWLEDGMENT .....	vi
LIST OF TABLES .....	ix
LIST OF FIGURES .....	x
LIST OF SYMBOLS .....	xi
LIST OF ABBREVIATIONS .....	xii
1. INTRODUCTION .....	1
2. ATOMISTIC SIMULATIONS OF SINGLE CHAIN AND BULK FLUORINATED POLYMERS .....	6
2.1. Molecular Model and Computational Methods .....	6
2.1.1. Molecular Dynamics .....	6
2.1.2. Minimization Methods .....	8
2.1.3. Semiempirical Approaches .....	9
2.2. Results And Discussion .....	12
2.2.1. Semiempirical Calculations .....	12
2.2.2. Molecular Dynamics Simulations of Bulk Systems of Fluorinated Polymers Under External Electric Field .....	17
3. MESOSCOPIC MORPHOLOGIES OF FLUORINATED OLIGOMERS IN AN APROTIC SOLVENT .....	23
3.1. Molecular Model and Computational Methods .....	23
3.1.1. Dissipative Particle Dynamics .....	24
3.1.2. Mesodyn .....	27

3.2. Results and Discussion .....	30
3.2.1. Interaction Energies and Parameterization .....	30
3.2.2. Mesoscale Calculations of The Fluorinated Polymers .....	35
3.2.2.1.Dissipative Particle Dynamics Simulations .....	35
3.2.2.2.Mesodyn Simulations .....	41
4. CONCLUSIONS AND SUGGESTIONS FOR FUTURE WORK .....	43
APPENDIX A: CONSISTENT FORCEFIELD-COMPASS .....	46
BIBLIOGRAPHY .....	48

## LIST OF TABLES

Table 3.1.	Beads used in the DPD and MesoDyn simulations .....	31
Table 3.2.	Solubility parameters and molar volumes of the beads .....	32
Table 3.3.	Flory-Huggins, conservative repulsion, and MesoDyn parameters .....	34
Table 3.4.	Interfacial tensions at different concentrations .....	40

## LIST OF FIGURES

Figure 2.1.	Evaluation of heats of formation of linear fluorinated polymer (a) long polymer chain and, (b) small polymer chain .....	13
Figure 2.2.	Predicted NMR shifts of (a) long and, (b) short chains .....	16
Figure 2.3.	Polarization vs. Electric field .....	18
Figure 2.4.	Views on the xy-plane of LFP40 system. Initial configuration before starting external electric field in the (a) +z direction and (b)-z direction; after applying electric field for 600 ps (c) +z direction and (d) -z direction .....	19
Figure 2.5.	Views on the xy-plane of LFP10 system. Initial configuration before starting external electric field in the (a)-z direction; after applying electric field for 600 ps (b) -z direction .....	20
Figure 2.6.	Views on the xy-plane of LFP20 system. Initial configuration external electric field in the (a)-z direction; after applying electric field for 600 ps (b) -z direction .....	21
Figure 3.1.	(a) Linear fluorinated polymer (b) Graft fluorinated polymer .....	24
Figure 3.2.	Radial distribution function .....	36
Figure 3.3.	Isosurface morphologies of linear fluorinated polymers at different concentrations (a) 20% in DMF (b) 30% in DMF (c) 40% in DMF (d) pure polymer .....	37
Figure 3.4.	Isosurface morphologies of graft fluorinated polymers at different concentrations (a) 20% in DMF (b) 30% in DMF (c) 40% in DMF (d) pure polymer .....	38
Figure 3.5.	RMS end-to-end distances of linear and graft fluorinated polymers .....	39
Figure 3.6.	Isosurface representations of the (a) Pure linear polymer (b) 20% Graft polymer .....	41

## LIST OF SYMBOLS

$\text{\AA}$	Angstrom
$k$	Boltzmann constant
$\epsilon_s$	Static dielectric constant
$E$	Energy of the system
$\chi_{AB}$	Flory-Huggins parameter
$N$	Number of atoms
$P$	Pressure
$\delta$	Solubility parameter
$T$	Temperature
$V_{bead}$	Molar volume of a bead
$\Psi$	Molecular orbital wave function

## LIST OF ABBREVIATIONS

AM1	Austin Model 1
AO	Atomic Orbital
CG	Conjugate Gradient
CI	Configuration Interaction
COMPASS	Condensed-phase Optimized Molecular Potentials for Atomistic Simulation Studies
DPD	Dissipative Particle Dynamics
FH	Flory-Huggins
HE	Half-Electron
GFP	Graft Fluorinated Polymer
LCAO	Linear Combination of Atomic Orbitals
LCAO-SCF	Linear Combination of Atomic Orbitals-Self Consistent Field
LFP	Linear Fluorinated Polymer
MC	Monte Carlo
MD	Molecular Dynamics
MNDO	Modified Neglect of Diatomic Overlap
MO	Molecular Orbital
PM3	Parametric Method Number 3
SCF	Self-Consistent Field
RDF	Radial Distribution Function
RHF	Restricted Hartree-Fock
RMS	Root Mean Square
SD	Steepest Descent

## **CHAPTER 1**

### **INTRODUCTION**

The discovery of polytetrafluoroethylene (PTFE) [Plunkett et al., 1960] induced new ideas for the synthesis of novel polymeric systems. PTFE is being used in many areas including pipes, valves, optical fibers, non-stick coatings for cookware, because of its special properties, such as low friction coefficient, low surface tension, and excellent chemical and thermal stability combined with excellent dielectric properties. Special properties of PTFE are due to its weak intermolecular forces and the strong C-F bonds. On the other hand, processing of PTFE is limited, because it is highly solvo-phobic. To improve solubility of fluorinated polymers in solvents, copolymer compounds with non-fluorinated moieties are synthesized. Therefore, the resultant copolymers are soluble and self-associated in solvents.

There are two different routes for synthesizing these interesting fluorinated polymers. The first way is the direct polymerization of fluorine-containing monomers. The other procedure is the modification of non-fluorinated parent polymers by incorporation of the fluorine atoms or fluorine-containing moieties to the polymer. There are different methods to incorporate fluorinated segments in polymers: (i) Participation of the fluorinated unit in the main chain, (ii) modification of polymer terminals by fluorinated derivatives, (iii) fluorination of side chains, and (iv) attaching fluorinated blocks to the non-fluorinated blocks [Bilgin et al., 2004].

Fluorinated surfaces derive their properties from C-F bonds, which have unique molecular properties. The chemical nature of the fluorinated compounds leads to specific, unique chemistry and physics at interfaces. Their low surface tension, low electrostatic loading, and low friction coefficient can play an important role in

microelectronic, antifogging and antifouling applications, and are promising in medical uses.

Studies show that increasing the  $\text{CF}_3$  concentration on the surface lowers the surface tension compared with  $\text{CF}_2$ -containing surfaces. This is attributed to the bulky fluorine atom leading to a lower density of attractive centers per unit area at the surfaces [Johnson et al., 1993]. It has been established that the surface tension depends on the constituent group and decreases in the order of  $\text{CH}_2$  (36 mN/m) >  $\text{CH}_3$  (30 mN/m) >  $\text{CF}_2$  (23 mN/m) >  $\text{CF}_3$  (15 mN/m). Furthermore, a uniformly ordered array of  $\text{CF}_3$  groups can create a surface with a surface tension as low as 6 mN/m [Zisman, 1964].

Studies show that the lowest surface tension can be attained by the self-assembled monolayers of perfluoroalkyl chains, where the surface is filled by a close-packed array of  $\text{CF}_3$  groups [Zisman, 1964]. Similar surface tension values are obtained by incorporating fluorinated monomers that are pendant to the parent polymer chain, such as partly-fluorinated polysiloxanes [Kobayashi et al., 1995; Thorpe et al., 1998; Perutz et al., 1996], polystyrenes [Höpken et al. 1992; Bouteiller et al., 1999; Kato et al., 1999], polyacrylates [DeSimone et al., 1992; Guyot et al., 1995; Ameduri et al., 2001; Morita et al., 1999], and polymethacrylates [Ameduri et al, 2001].

Several research groups have reported polymer systems exhibiting a low surface tension by grafting perfluoroalkyl groups to polymer chains [Hwang et al., 1995; Perutz et al., 1996; Park et al., 1997]. Other polymer architectures, like end-functionalized polymers [Albert et al., 1984] and block copolymers [Wang et al., 1997] have also been employed to obtain fluorinated polymer surfaces with low surface tensions.

Investigations of surface structures and surface properties of polymeric systems have been carried out extensively, both experimentally [Chaudhury et al., 1992] and theoretically [Jones et al., 1999]. In accordance with the specific surface properties of fluorinated polymeric materials, continuing efforts have been made towards the understanding of the relation between the microscopic surface structure and the macroscopic surface properties. It is well known that some of the important factors for low surface tensions include both the precise nature of the atomic population at the surface and their physical arrangement. However, the search for a correlation has often

been impeded by a missing link, namely, the knowledge of the composition in the outermost atomic layer. One of the novel nanofiber manufacturing processes is the electrospinning in which a high voltage is applied to a capillary filled with the polymer fluid to be spun. Electrospinning method has been recently applied to several fluorinated polymers to generate superhydrophobic surfaces [Acatay et al., 2004].

Complex fluids can be described as those in which the observable behaviour is affected in a fundamental way by the microscopic structure of the fluid [Cohen, 1962]. Complex fluids are used in many areas; paper manufacturing, coating processes, paints, food products, and medicine bioparticulates (including blood cells). There are many theoretical studies on these systems, but prediction of experimental results is difficult and computer power is insufficient due to the time and length scale problems. Physical phenomena occur on macroscopic length and time scales, while the fundamental causes of these phenomena can occur on the scale of the complex fluid elements themselves [Bird et al., 1987; Ferrante, 1996; McLeish, 1997].

In most cases, simple fluids can be adequately described by Navier-Stokes type equations [Batchelor, 1992] and several sophisticated computational methods of these equations at the macroscopic level have been established. These methods, on the other hand, can include the microscopic details of the fluid only to estimate the macroscopic properties and are therefore not suitable for the many complex fluid systems. Another method, Molecular Dynamics [Alder and Wainwright, 1957], at the microscopic scale, is used for the simulation of liquids by following the position and momentum of every particle in the fluid. Although this method has become increasingly successful in the simulation of a small number of particles, its application to the complex fluid systems mostly result in unrealistic computational demands.

Mesosopic simulation methods [Boghosian et al., 1997] have been established to circumvent the inherent difficulties faced by traditional methods when applied to complex fluids. The first method at this scale is the lattice gas approach [Doolen, 1990; Frisch et al., 1986] in which discrete particles move on a grid in accordance with a particular set of collision rules. This method allows predicting empirical modeling of immiscible fluids [Rothman and Keller, 1988; Rothman and Zaleski, 1994]. The

alternative improved model is the Lattice Boltzmann model that uses distribution functions defined on a grid.

A new method, Dissipative Particle Dynamics (DPD), was originally developed by Hoogerbrugge and Koelman in 1992 [Hoogerbrugge et al., 1992] and is a mesoscopic fluid simulation technique that was designed to facilitate the simulation of static and dynamic properties of complex fluid systems on physically interesting length and time scales. Unlike many other mesoscopic methods, the DPD system exists in continuous space, rather than on a lattice. The DPD method can be defined as bridging the gap between microscopic simulation methods, and the macroscopic approaches. In this method, a collection of particles move according to Newton's equations of motion. Since the inter-particle interactions are softly repulsive, longer time-scales can be used compared with MD method.

Another method, developed for the simulation of complex fluids, is MesoDyn [Altevogt et al., 1999], where the dynamics of the system is described by a set of so-called functional Langevin equations. These equations are simply diffusion equations in the component densities, which take account of the noise in the system. Starting from an initially homogenous mixture of the mesoscale box, the evolution of the component density is simulated. MesoDyn has been used for the simulation of 2D and 3D phase separation of immiscible fluids [Fraaije et al., 1997; Maurits et al., 1998; Zvelindovsky et al., 1998].

In this thesis, simulations are made to the fluorinated polymers at the quantum mechanical level as well as the atomic, and mesoscopic scales. Polymers chosen in this study were synthesized by Bilgin et al. [2004] to study their phase behaviour. As mentioned above, fluorine containing materials have high contact angle with water and low surface energy. Electrospun fibers of fluorinated polymers show higher contact angles compared to cast films [Acatay et al.]. This result attracts our interest to investigate the effect of electric field on the conformational properties of fluorinated polymers. Thus, we studied the phase behaviour of linear fluorinated polymers in the presence of a strong electric field. We also performed semiempirical calculations on linear fluorinated polymers and calculated various properties, such as  $^{13}\text{C}$  chemical shifts, heats of formation, dipole moments, and Mulliken atomic charges.

In the industrial applications of polymers, understanding mesoscale structures are essential for predicting the macroscopic properties of these materials. In this thesis, graft and linear chains of fluorinated polymers at different concentrations in dimethylformamide (DMF), and in vacuum are simulated by Dissipative Particle Dynamics and MesoDyn [Accelrys Inc]. Polymer-solvent phase separation of the system has also been studied.

## **CHAPTER 2**

### **ATOMISTIC SIMULATIONS OF SINGLE CHAIN AND BULK FLUORINATED POLYMERS**

#### **2.1.Molecular Model and Computational Methods**

In this part, we outline single chain and bulk simulations of linear ABCBA type fluorinated polymers where **A** segment is hydrophobic ( $-C_6F_{13}$ ) and, **B** and **C** segments are hydrophilic ( $-CH_2CH_2OCOCH_2CH_2-$ ) and ( $-CH_2CH(CN)-$ ), for **B** and **C** respectively. All simulations are performed on a PC (with 1.60 GHz CPU and 524 mega Bytes RAM). Semiempirical calculations and MD simulations are made using VAMP [Clark et al, 2002] and Discover modules of the Materials Studio program [Accelrys Inc], respectively.

##### **2.1.1. Molecular Dynamics**

MD simulations provide the molecular level picture of structure and dynamics and it is one of the most useful methods, giving information about structure-property relationships. Experiments often do not provide the molecular level information available from simulations; therefore, theoreticians and experimentalists can have synergistic relationships that lead to new insights into material properties. MD simulations allow prediction of properties for novel materials which have not been synthesized, as well as existing materials whose properties are difficult to measure or poorly understood.

MD is a numerical integration of the classical equations of motion, thus successive configurations of the system are generated in time. MD simulations provide a trajectory, in which positions and velocities of the atoms vary with time. Newton's laws of motion are used in the theory of MD simulations and the trajectory is obtained by solving the differential equations of Newton's second law:

$$\mathbf{F}_i = m_i \mathbf{a}_i \quad (2.1)$$

where  $\mathbf{F}_i$  is the force exerted on particle  $i$ , and  $m_i$  and  $\mathbf{a}_i$  are the mass and acceleration of particle  $i$ , respectively. However, the force acting on particle  $i$  can also be expressed as the gradient of the potential energy,  $V$ :

$$\mathbf{F}_i = -\nabla_r V \quad (2.2)$$

Equations (2.1) and (2.2) yield:

$$-\frac{dV}{d\mathbf{r}_i} = m_i \frac{d^2 \mathbf{r}_i}{dt^2} \quad (2.3)$$

where the potential governing the motion of particle  $i$  is the sum over all the effective interactions and is generally called a forcefield. Newton's equations of motion can then relate the derivative of the potential energy to the changes in position as a function of time. COMPASS forcefield [Sun, 1998] used in this study has been shown to be very effective in defining properties of synthetic polymers (Appendix A). The potential is a function of the atomic positions of all the atoms in the system and due to the complicated nature of this function, there is no analytical solution to the equations of motion, thus they are solved numerically. The velocity Verlet algorithm is used to integrate Equation 2.3 to yield position vectors at a given time using the forces and previous positions of the atoms [Verlet, 1967].

An MD simulation generates a sequence of points in phase space as a function of time, where these points belong to some ensemble. They correspond to the different conformations of the system and the respective momenta. The main types of ensembles used are:

- (i) Microcanonical Ensemble ( $NVE$ ): The thermodynamic state characterized by a fixed number of atoms,  $N$ , a fixed volume  $V$ , and a fixed energy,  $E$ . This corresponds to an isolated system.
- (ii) Canonical Ensemble ( $NVT$ ): This is a collection of all systems whose thermodynamic state is characterized by a fixed number of atoms,  $N$ , a fixed volume,  $V$ , and a fixed temperature,  $T$ .
- (iii) Isobaric Ensemble ( $NPT$ ): This ensemble is characterized by a fixed number of atoms,  $N$ , a fixed pressure,  $P$ , and a fixed temperature,  $T$ .
- (iv) Grand Canonical Ensemble ( $\mu VT$ ): The thermodynamic state for this ensemble is characterized by a fixed chemical potential,  $\mu$ , volume and temperature.

The equilibration of the systems to make the relevant properties to converge to their equilibrium values is an important factor. Simulation time depends on the size of the system and the computer power. Simulations on a small part of the system may give misleading results; on the other hand, simulation of the whole system for long times is beyond the accessible computer power. For polymeric systems in liquid or crystalline environment, this contradiction can be eliminated partly by using periodic boundary conditions. This method is cleverly developed and only hundreds or thousands of atoms behave as if they move in an infinite-sized bulk system. Periodic boundary conditions also remove the effects of the surface [Allen and Tildesley, 1989]

### **2.1.2. Minimization Methods**

There are several minimization methods implemented in Discover program [Accelrys Inc.]. By default, the smart minimization method, which automatically combines appropriate features of the available methods in a cascade, is used. The smart minimizer starts with the steepest descent method (SD), followed by the conjugate

gradient method (CG) and ends with a Newton Method. In our simulations all the structures are minimized by smart minimization method before further calculations.

SD is the method most likely to converge, no matter what the function is or where it begins. This method will quickly reduce the energy of the structure during the first few iterations. However, convergence will slow down considerably as the gradient approaches zero, therefore it should be used when the gradients are very large and the configurations are far from the minimum. It is typically used for poorly refined crystallographic data, or for graphically built molecules.

CG improves the line search direction by storing information from the previous iteration. It is used for large systems, where storing and manipulating a second-derivative matrix is difficult. Time interval of the iteration is longer than SD, but this is more than compensated for by efficient convergence. Fletcher-Reeves [Fletcher et al., 1964] and Polak-Ribiere [Polak et al., 1974] algorithms can be used for this method.

Since Newton methods require computation and storage of second derivatives, they are expensive in terms of computer resources. The Newton-Raphson method is only recommended for systems with a maximum of 200 atoms. It has a small convergence radius but it is very efficient near the energy minimum. Discover program supports three other variants on the Newton methods. The BFGS (Broyden, Fletcher, Goldfarb, and Shanno [Fletcher, 1980]) and DFP (Davidon, Fletcher, and Powell [Powell, 1977]) quasi-Newton algorithms use an update formula to simulate a second-derivative matrix. Truncated Newton combines the strengths of the conjugate gradient and Newton-Raphson methods.

### **2.1.3. Semiempirical Approaches**

In the semiempirical molecular orbital (MO) theory, some parameters are obtained to reproduce experimental results. Semiempirical techniques use the same Linear Combination of Atomic Orbitals-Self Consistent Field (LCAO-SCF) theory as *ab initio* methods. However, many of the more complex integrals used in the solution of

Schrödinger equation are ignored or approximated. To compensate the errors introduced by removing the integrals, empirical parameters and functions are used. These empirical parameters are fitted to reproduce experimental data. To increase accuracy of the empirical parameters, a large and varied training set of molecules should be considered. It has been used with different approximations to different types of molecules, starting from Pople's study in the 1950s and 1960s, e.g. MNDO, AM1, PM3 [Dewar et al., 1977 and 1985; Stewart, 1989].

The electron positions in molecular orbitals can be approximated by a linear combination of atomic orbitals, so this reduces the problem of finding the best functional form for the molecular orbitals to the much simpler one of optimizing a set of coefficients ( $c_n$ ) in a linear equation:

$$\Psi = c_1\phi_1 + c_2\phi_2 + c_3\phi_3 + c_4\phi_4 + \dots \quad (2.4)$$

where  $\Psi$  is the molecular orbital wave function and  $\phi_n$  represent atomic orbital wave functions.

Slater-type atomic orbitals are used in semiempirical methods rather than Gaussian functions. Although the Slater functions are much more difficult to solve exactly than Gaussian functions, they represent the electron density far from the nucleus better. Two-electron integrals can be evaluated using multipole approximations by Slater functions, rather than an exact calculation.

Molecular orbitals can then be built up by an iterative procedure that optimizes the LCAO coefficients,  $c_n$ . This variational self-consistent field (SCF) method is based on Hartree-Fock-Roothan-Hall theory [Marder, 2000], and constitutes the main part of most MO programs. Once the wave function is determined, many properties of the molecule can be calculated, such as the energy of the molecule, the atomic forces and other electronic properties. The energy and the atomic forces are used to optimize the geometry of the molecule to a stationary point (usually a minimum or a transition state) at which the atomic forces are ideally all zero.

Semiempirical methods are generally used for molecules that are too large for geometry optimization at the Hartree-Fock split-valence level of *ab initio* theory or with comparable basis sets with density functional theory (DFT). Molecules in the range of 50 to 400 atoms can be treated by semiempirical MO theory, but these numbers may increase as the computer power improves. In general, molecules larger than this range should be investigated by forcefield methods or mixed QM/MM calculations, and the smaller ones by *ab initio* methods or density functional theory.

Since semiempirical methods reproduce experimental results and larger molecules can be treated compared to other quantum mechanical methods, it has many usages in industry and application oriented research, such as (i) fast calculation of optimized geometries and molecular orbitals, (ii) transition state searching and optimization, (iii) calculation of accurate and reliable molecular electrostatic properties, potentials, and fields, (iv) calculation of spectroscopic properties including ESR, NMR, IR, and Raman frequencies, together with hyperpolarizabilities for nonlinear optical studies, (v) investigation of solvent effects and solvochromatic shifts, (vi) simulation of the environment using a mixed quantum mechanical and classical mechanical model.

In this study, AM1 (Austin Model 1) that is an *s* and *p* orbital based MNDO-like method is used. Yet, it differs from MNDO in that extra Gaussian potentials are added to the core-core repulsion energy to allow it to form hydrogen bonds. AM1 has been parameterized for most of the main group elements (e.g. H, B, C, N, O, F, Na, Mg, Al, Si, P, S, Cl, Br, I, Zn, Ge, Sn, Hg). Heats of formation can be predicted more successfully by AM1 than MNDO. Among the *s* and *p* orbital based methods, AM1 underestimates bond torsion barriers the least, and is therefore the method of choice for many applications involving  $\pi$ -systems, including amides. AM1 is a good method for the organic molecules and peptides, while it is not recommended for the compounds containing phosphorus and sulfur.

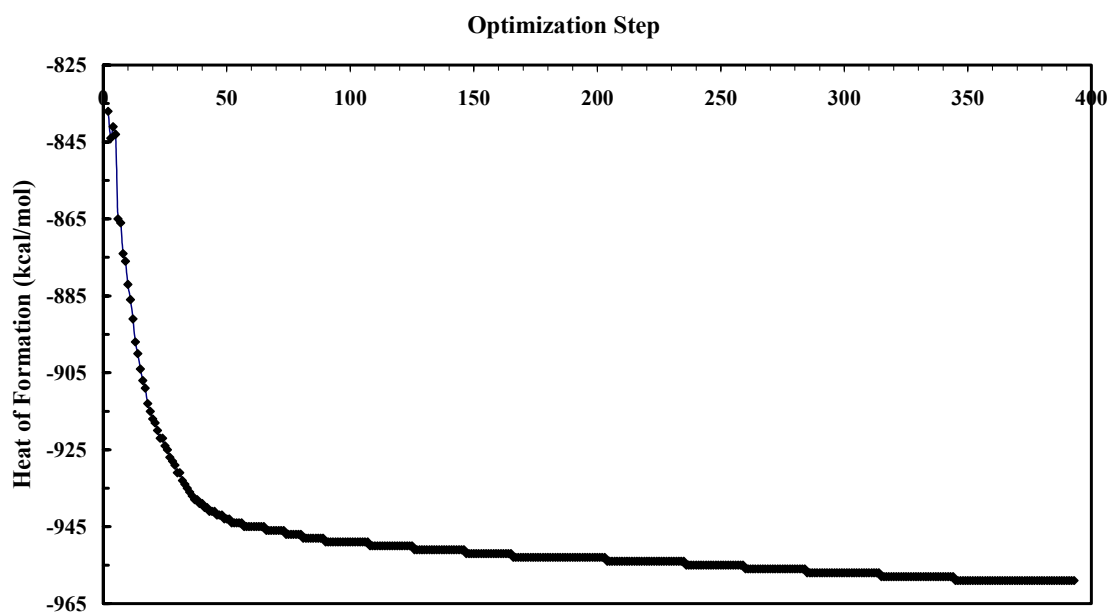
## 2.2.Results and Discussion

### 2.2.1. Semiempirical Calculations

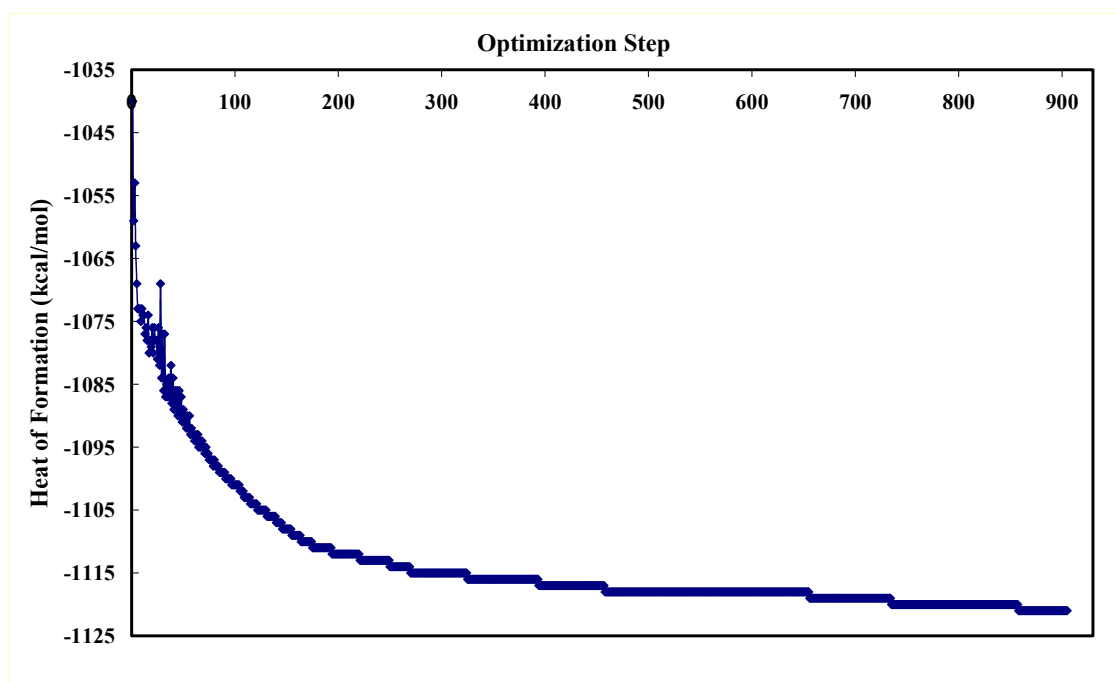
For the semiempirical calculations, two linear fluorinated polymers of type ABCBA that are different in length are used. The long and short polymers have 18 and 10 repeating units of acrylonitrile (-CH<sub>2</sub>CH(CN)-) in the middle, respectively. Polymers were built in Materials Studio and smart minimization was used for 20,000 steps. The convergence criterion is set to 10<sup>-4</sup> kcal/mol. For all semiempirical calculations the AM1 method is used. Charge and spin multiplicity is set to 0 and 1, respectively. Semiempirical calculations were directly performed on the long polymer chain after minimization, while high temperature MD simulations were carried out on the short chain before further calculations.

Evaluating the semiempirical energy expression requires VAMP to solve a set of coupled equations self-consistently. This results in a description of the average field that each electron experiences, i.e. the SCF approximation. All calculations involve at least one SCF calculation. In our study, Restricted Hartree-Fock (RHF) method is used as a SCF procedure. In a RHF calculation, only one set of molecular orbital is calculated, and this is constrained to be either doubly occupied or empty. A Half-Electron (HE) calculation is really a RHF calculation in which the unpaired electron is represented by two-paired half electrons. HE and RHF calculations are the basis for the Configuration Interaction (CI) calculations performed by VAMP. HE geometry optimizations can be slow, or even fail, because the electron pairing correction to the energy may cause errors in the atomic forces. Usually, in RHF calculation, each occupied MO contains two electrons. In an HE calculation, this is not the case.

VAMP [Clark et al., 2002] calculates many properties, such as heats of formation, dipole moments, static polarizabilities, and <sup>13</sup>C shifts. For the long linear polymer, in which all the backbone dihedral angles are in the range of 110 degree, evaluation of the heats of formation is shown in Figure 2.1.a and is found as -968 kcal/mol.



(a)



(b)

**Figure 2.1.** Evaluation of heats of formation of linear fluorinated polymer (a) long polymer chain and, (b) small polymer chain.

The initial structure of the second (short) linear polymer is taken from the result of the high temperature MD simulations. In this structure,  $-\text{CH}_2\text{CH}(\text{CN})-$  is repeated ten times. High temperature MD is a very useful method for the conformational search analysis and gives very efficient results for its purposes [Baysal et al., 1999]. According to this procedure, first an MD simulation is carried out at high temperature, and various structures are recorded during the run. The high temperature MD ensures that the generated structures sample a wide range on the potential energy surface. So, high energy barriers are easily surmounted, preventing the search from being stuck in a given energy well. The recorded structures are subsequently minimized by the smart minimization method. Finally, the energy-minimized structures are arranged in order of energy and only the structures that are significantly different from each other are retained. We can get information about the characteristics of the potential energy surface from the minimized structures, especially the low energy wells.

In this study, we first randomly generated a fluorinated polymer chain with a block of 10 repeat units of acrylonitrile in the middle. Dihedral angles were in the range of  $100-120^\circ$ . We next carried out MD simulations at 1000 K treating all atoms explicitly. A time step of 1 fs was used, and the temperature was fixed at 1000 K by using the temperature control method of Andersen [Andersen, 1980]. Initial velocities were generated from a Boltzmann distribution with an average temperature of 1000 K. Integration was carried out by the velocity Verlet algorithm. Atom-based cutoffs were used with a  $12.5 \text{ \AA}$ ; a switching function was used with the spline and buffer widths set to 3 and  $1 \text{ \AA}$ , respectively. The neighbour list was updated whenever any atom moved more than one-half of the buffer width. High temperature MD was carried out for 1 ns and atomic positions were saved every 1000 steps, yielding 1000 structures. Then smart minimization was made on the resultant structures for 20000 steps. The conformation that has the least energy was chosen for further semiempirical calculations. The same semiempirical parameters as in the long one are used for this polymer, and evaluation of the heat of formation (Figure 2.1b) and theoretical  $^{13}\text{C}$  chemical shifts (Figure 2.2b) are calculated.

Since the long and small polymer chain has 59 and 43 dihedral angles, respectively, geometry optimization by semiempirical methods cannot span the entire

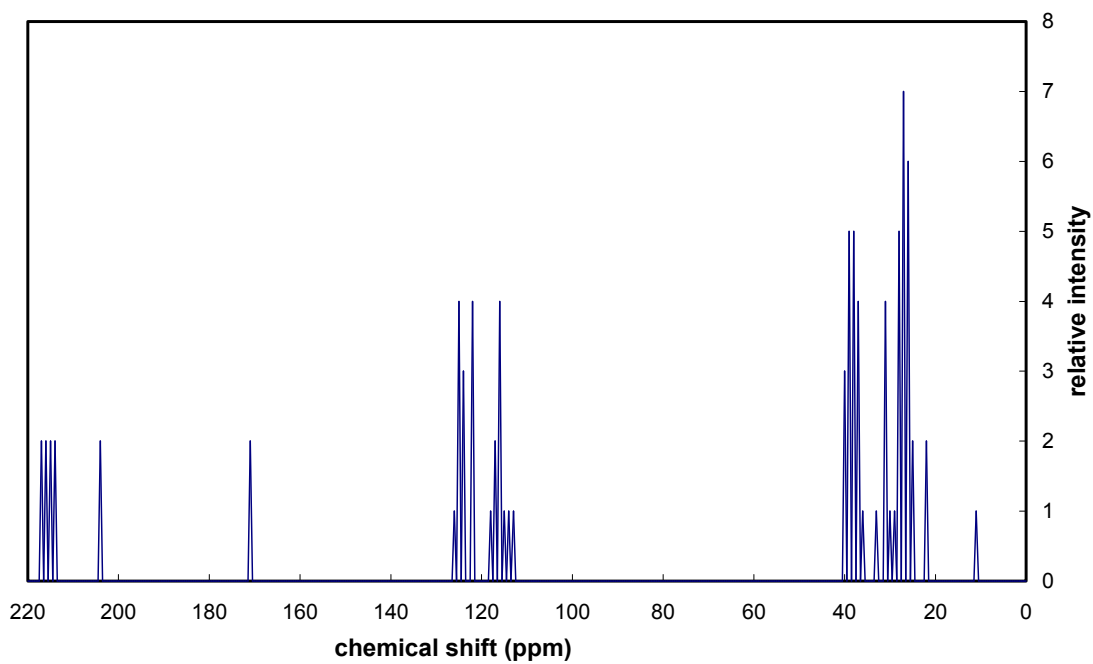
potential energy surface. For example, cartesian coordinates of the atoms of the long polymer chain does not change and also all the dihedral angles stay in the same range.

High temperature MD simulation of short polymer chain ended with a U-shaped structure. After treatment with semiempirical method, there wasn't a significant change in the dihedral angles. Although, semiempirical methods can be used for the systems containing upto 400 atoms; it does not optimize structures, which have many dihedral angles as in our case, to its global minimum.

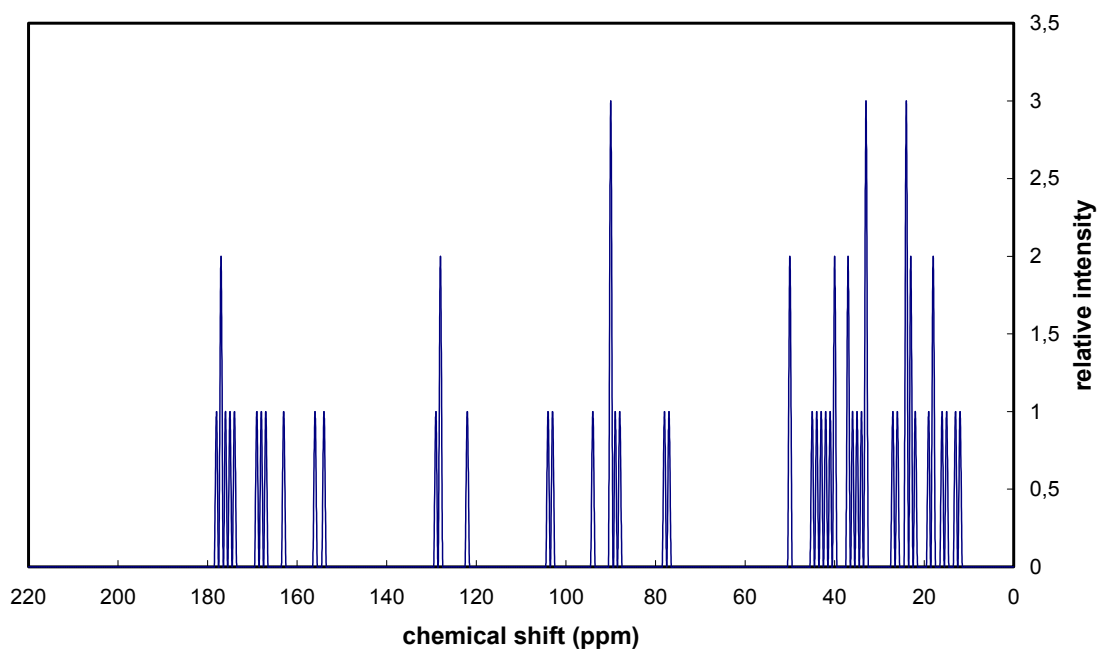
Theoretical  $^{13}\text{C}$  NMR shifts [Clark et al., 1995] can be calculated from the simulation (Figure 2.2). The spectrum can be analyzed starting from referenced carbon chemical shifts.  $^{13}\text{C}$  chemical shifts of the long polymer chain are populated in three intervals, which are 20-40, 110-130 and, above 200 ppm. The first chemical shift range corresponds to the carbon atoms in  $\underline{\text{C}}\text{-CN}$ ,  $\text{R-OC(O)-}\underline{\text{C}}$ . The chemical shifts between 110 and 130 are due to the carbon atoms bonded to the fluorine atoms. The larger chemical shifts are corresponding to the ester carbon atoms [Lambert et al., 1997].

The small chain has a wider range of chemical shifts, so interpretation is difficult, but typical chemical shifts are also observed. For example, chemical shifts corresponding to carbon in  $\underline{\text{C}}\text{-F}$  are mediated around 80-100 ppm. The wide range of the spectrum can be due to the coiled structure of this chain in which neighbouring atoms increases and coupling effects also comes into play. In the long polymer case the structure is almost linear, so the coupling effects from the non-bonded atoms do not appear.

NMR spectra provide information about the conformation or average conformation of the fluorinated polymers. Since the short polymer has wide spectrum it is more realistic and in the third chapter, we also found that the rms end-to-end values verify the short polymer structures is more realistic.



(a)



(b)

**Figure 2.2.** Predicted NMR shifts of (a) long and, (b) short chains

### 2.2.2. Molecular Dynamics Simulations of Bulk Systems of Fluorinated Polymers Under External Electric Field

In the presence of an external electric field,  $E$ , the force experienced by a unit charge  $q$  is:

$$F = qE \quad (2.5)$$

The relationship between the polarization  $P$  induced in a material by an external electric field (that is, the total dipole moment per unit volume) and the field is given by:

$$\epsilon_s - 1 = 4\pi \frac{P}{E} \quad (2.6)$$

where  $\epsilon_s$  denotes the static dielectric constant.

The effect of the external electric field on the configurations of the linear fluorinated polymers (LFP) is investigated in this section. Three simulation boxes are constructed at different sizes and densities and initially 2000 step of smart minimization is made on each system. The first system consists of 40 chains of fluorinated polymers (denoted by LFP40) and its density is set to 1 g/cm<sup>3</sup>. The second (denoted by LFP10) and third simulation (denoted by LFP20) boxes have 10 chains with density 1.2 g/cm<sup>3</sup> and 20 chains with density 0.5 g/cm<sup>3</sup>, respectively. The box sizes are set to 41×41×16 Å for LFP10, 90×90×16 Å for LFP40, and 90×90×16 Å for LFP20. The box sizes are set to smaller values in the  $z$  dimension, because electric field is applied in  $+z$  direction.

MD simulations on the three systems, under external electric field were carried out on all systems at 298 K, treating all atoms explicitly. A time step of 1 fs was used, and the temperature was kept fixed at 298 K by using the temperature control method of Andersen [Andersen, 1980]. Initial velocities were generated from a Boltzmann distribution with an average temperature of 298 K. Integration was carried out by the velocity Verlet algorithm [Verlet, 1967]. Atom-based cutoffs were used with 8.5 Å cutoff

distance; a switching function is used with the spline and buffer widths set to 1.0 and 0.5 Å, respectively. The neighbor list is updated whenever any atom moves more than one-half the buffer width. The systems were equilibrated for 5 ps under zero electric field, and further simulated for 600 ps with an external field in the +z direction. Electric field is set to  $1 \times 10^7$  eV/m for the first 200 ps period,  $1 \times 10^9$  eV/m for the following 200 ps, and  $1 \times 10^{11}$  eV/m for the last 200 ps. Polarization increases as the electric field is increased (Figure 2.3.).

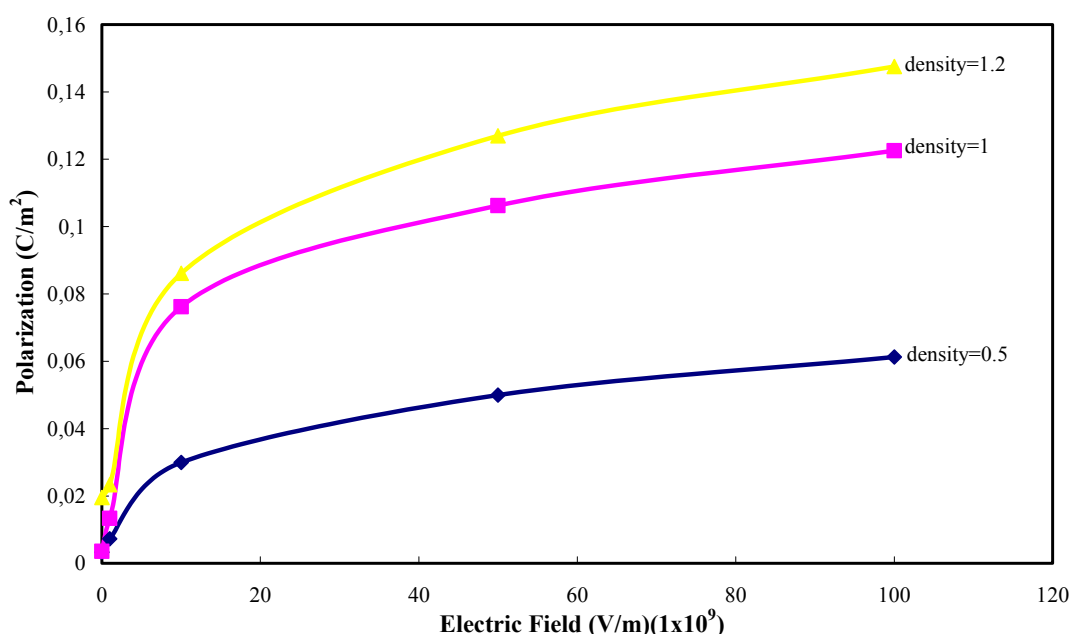


**Figure 2.3.** Polarization vs. Electric field

In all three systems, polarization increases with external electric field. The main structural unit causing the increase in polarization is the polar  $-CN$  group. The other interesting thing is that the polarization also increases with the density. This is obviously, because of increasing cyanide content. The dynamic evolution of the alignments of the polymer chains can be investigated using trajectory files. Two dimensional views of the systems are shown in Figures 2.4, 2.5, and 2.6. The N atoms are shown in blue, F atoms in cyan, C atoms in gray and H atoms in white.

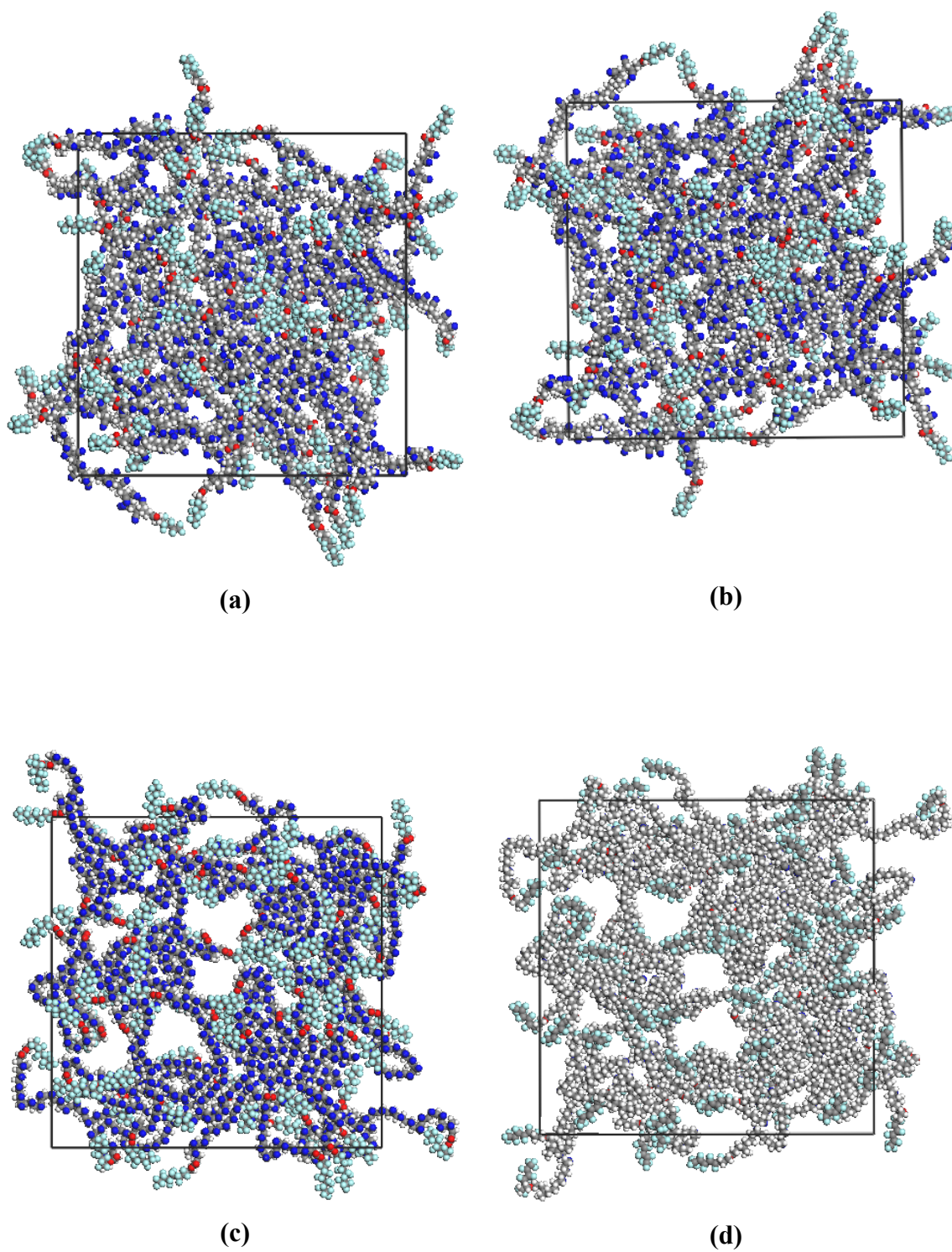
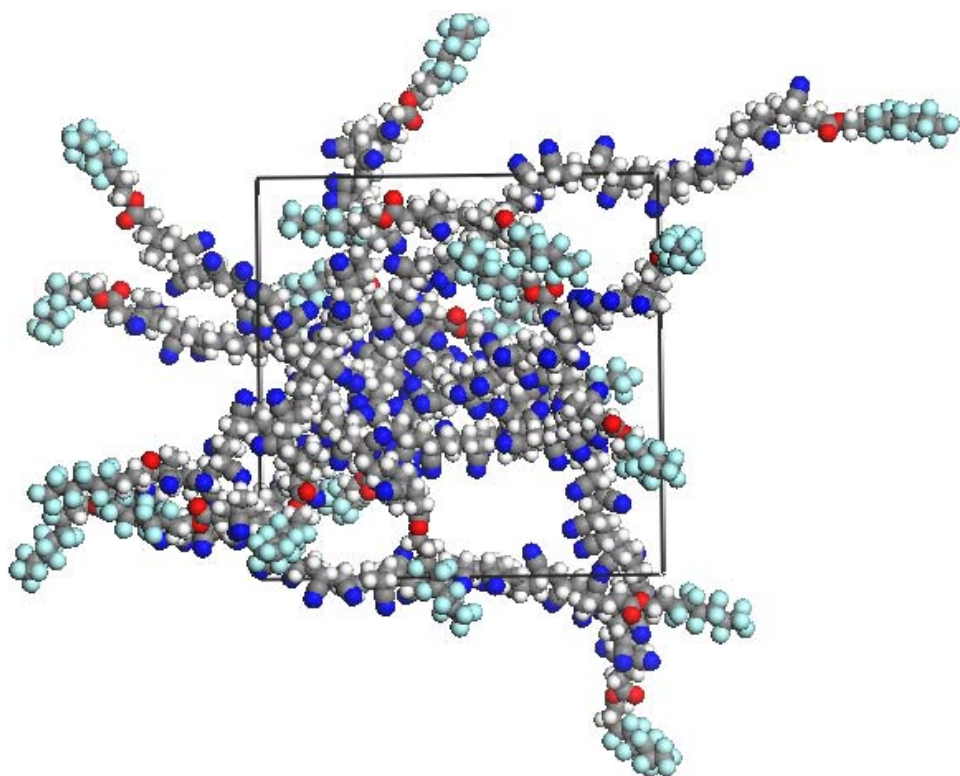
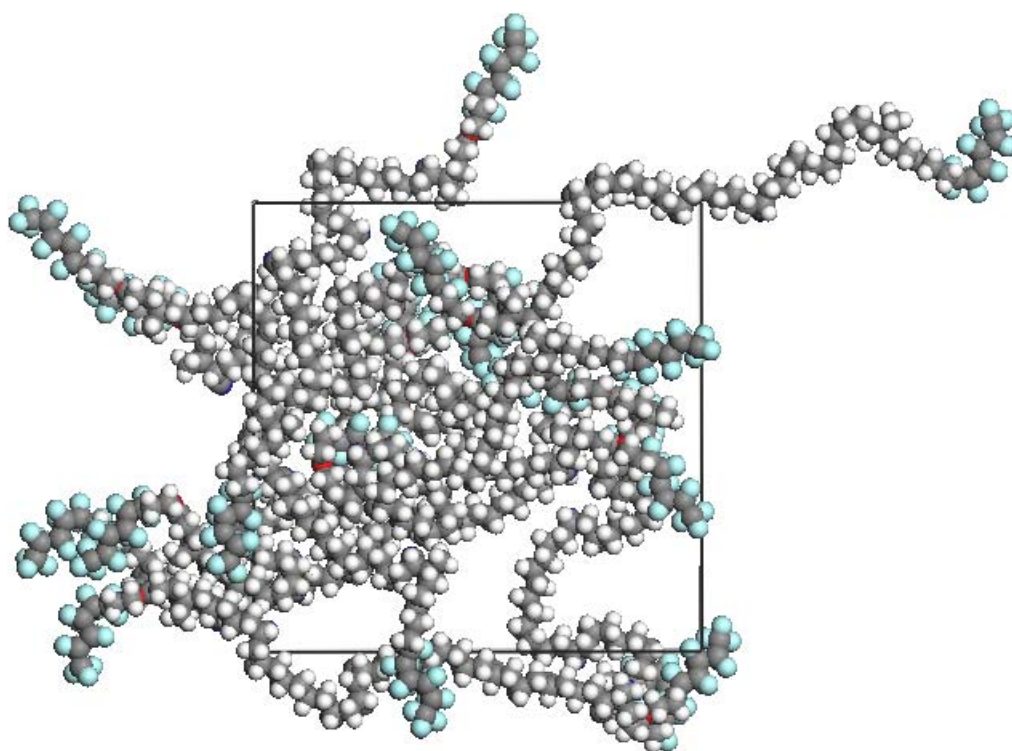


**Figure 2.4.** Views on the xy-plane of LFP40 system. Initial configuration before starting external electric field in the **(a)** +z direction and **(b)**-z direction; after applying electric field for 600 ps **(c)** +z direction and **(d)** -z direction.

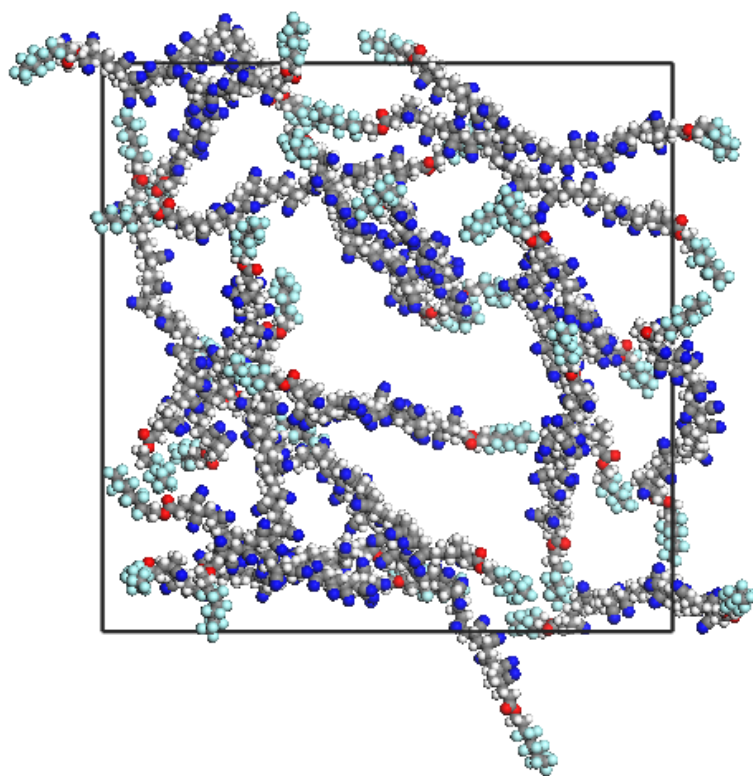


(a)

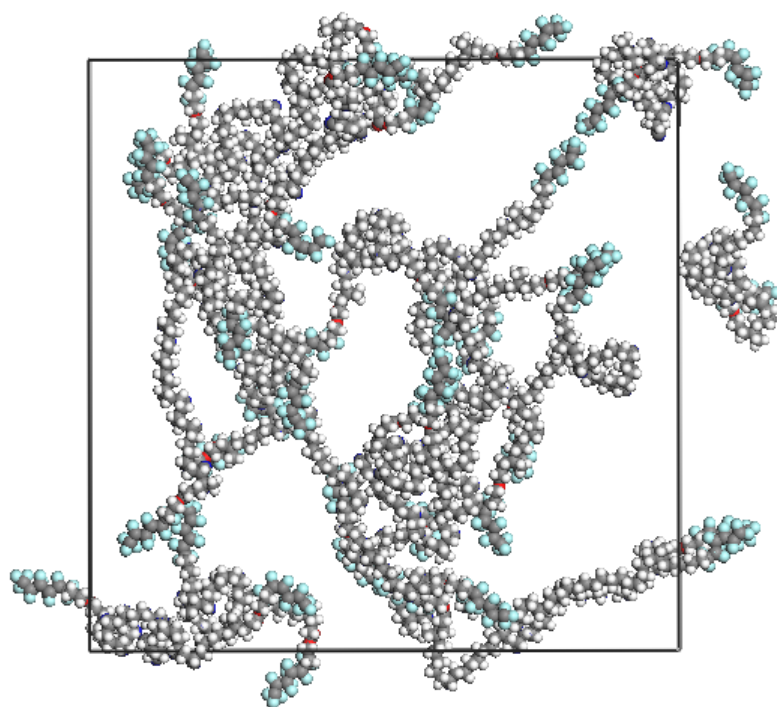


(b)

**Figure 2.5.** Views on the xy-plane of LFP10 system. Initial configuration before starting external electric field in the (a)-z direction; after applying electric field for 600 ps (b) -z direction.



(a)



(b)

**Figure 2.6.** Views on the  $xy$ -plane of LFP20 system. Initial configuration external electric field in the (a)- $z$  direction; after applying electric field for 600 ps (b)  $-z$  direction.

As mentioned, polarity of the  $-\text{CN}$  group causes the increase in the polarization with applied external electric field. Alignment of the  $-\text{CN}$  groups along the  $+z$  direction starts after applying electric field. We observed that the total alignment can be obtained only after applying  $1 \times 10^{11}$  eV/m. At low external fields partial alignments occur.

Since the apolar fluorine containing blocks are not affected by the external electric field, chain conformations are reorganized so as to increase the fluorine content of the simulation box on the opposite face of the direction of electric field. If we consider the simulation box as a thin film, fluorine content can be increased by applying external electric field. This may be useful for the design of fluorine-rich surfaces.

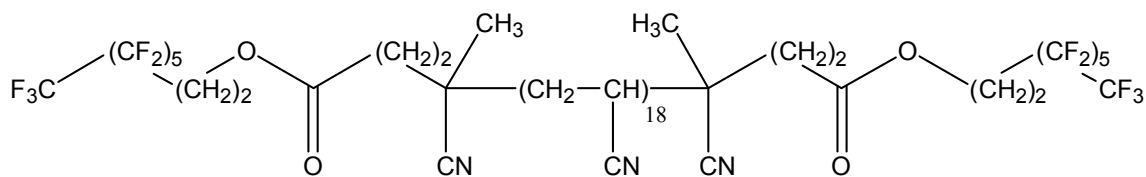
## CHAPTER 3

### MESOSCOPIC MORPHOLOGIES OF FLUORINATED OLIGOMERS IN AN APROTIC SOLVENT

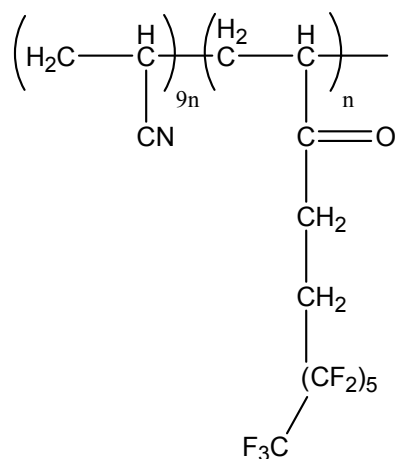
#### 3.1. Molecular Model and Computational Methods

In this study two fluorinated oligomers, typical of those synthesized by the Menciloglu group [Bilgin et al., 2004], are used for the mesoscale calculations. The ABCBA type linear chain (Figure 3.1a) is produced by using fluorinated initiators. **A** blocks are CO<sub>2</sub>-philic blocks of C<sub>6</sub>F<sub>13</sub>. **B** and **C** are CO<sub>2</sub>-phobic blocks of ethyl propionate -(CH<sub>2</sub>)<sub>2</sub>OCO(CH<sub>2</sub>)<sub>2</sub>- and 18 repeat units of -CH<sub>2</sub>CH(CN)- (acrylonitrile), respectively. The second fluorinated polymer has the same blocks, but with the **BA** blocks grafted to the **C** backbone. The **C:BA** block ratio is 10 (Figure 3.1b). Mesoscopic morphologies of fluorinated oligomers are investigated in dimethylformamide (DMF) at different concentrations.

All the simulations were performed on a PC (with 1.60 GHz CPU and 524 mega Byte RAM), and the DPD, MesoDyn, Discover, Amorphous Cell modules in Materials Studio 2.2. software package from Accelrys Inc. are used. COMPASS (Appendix A) forcefield was used for the MD simulations and graphical displays were generated with the Materials Visualizer.



(a)



(b)

**Figure 3.1.** (a) Linear fluorinated polymer (b) Graft fluorinated polymer.

### 3.1.1. Dissipative Particle Dynamics

The mesoscopic simulations are very important for understanding complex fluid dynamics. Dissipative Particle Dynamics (DPD), developed by Hoogerbrugge and Koelman [Hoogerbrugge et al., 1992], has been improved by Groot and Warren [Groot et al., 1997]. In this method, mesoscopic regions of fluid material that show similar chemical properties are represented by fundamental particles called “beads.” Contrary to MD, these particles do not have atomic properties since all degrees of freedom smaller than a bead radius are assumed to have been integrated out. Thus, coarse-grained interactions between beads are calculated, and all atomic details are lost.

DPD simulations are performed on a collection of particles interacting with Newton's equations of motion.

$$\frac{d\mathbf{r}_i}{dt} = \mathbf{v}_i, \quad \frac{d\mathbf{v}_i}{dt} = \mathbf{f}_i \quad (3.1)$$

The reduced masses are set at 1, so the force acting on a particle equals to its acceleration. There are three contributions to the overall force acting on the  $i$ th particle. These short-range inter-particle forces are (i) a repulsive conservative force  $\mathbf{F}_{ij}^C$ , (ii) a dissipative force  $\mathbf{F}_{ij}^D$ , (iii) and a random force  $\mathbf{F}_{ij}^R$  acting symmetrically between every pair of particles  $i$  and  $j$ :

$$\mathbf{f}_i = \sum_{j \neq i} (\mathbf{F}_{ij}^C + \mathbf{F}_{ij}^D + \mathbf{F}_{ij}^R) \quad (3.2)$$

where the sum runs over all particles within a certain cutoff radius  $r_c$  of the  $i$ th bead. This short-range cutoff makes the interactions local. For simplicity, the cutoff radius is taken as unity, since this is the only length-scale in the system. Therefore, all forces beyond the bead radius cancel. Soft repulsion interactions are considered, and the excluded-volume effect is not operative.

The repulsive conservative force  $\mathbf{F}_{ij}^C$  acts along the centers of the  $i$ th and  $j$ th particles, as:

$$\mathbf{F}_{ij}^C = \begin{cases} a_{ij}(1-r_{ij})\hat{\mathbf{r}}_{ij} & (r_{ij} \leq 1) \\ 0 & (r_{ij} \geq 1) \end{cases} \quad (3.3)$$

where  $a_{ij}$  is the maximum repulsion between particles  $i$  and  $j$ ; and  $\mathbf{r}_{ij} = \mathbf{r}_i - \mathbf{r}_j$ ,  $r_{ij} = |\mathbf{r}_{ij}|$ ,  $\hat{\mathbf{r}}_{ij} = \mathbf{r}_{ij}/|\mathbf{r}_{ij}|$ .

The dissipative force  $\mathbf{F}_{ij}^D$  depends on the relative velocity of two beads and acts to reduce their relative momentum:

$$\mathbf{F}_{ij}^D = -\gamma\varpi^D(r_{ij})(\hat{\mathbf{r}}_{ij}\mathbf{v}_{ij})\hat{\mathbf{r}}_{ij} \quad (3.4)$$

where  $\varpi^D(r_{ij})$  is a short-range weight function. Because of the form chosen for the dissipative force, the total momenta of each pair of particles, and consequently that of the overall system are conserved.

The random force also acts between all pairs of beads subject to a similar short-range cutoff, but a different distance-dependent  $\varpi^R(r_{ij})$  is used:

$$\mathbf{F}_{ij}^R = \sigma\varpi^R(r_{ij})\theta_{ij}\hat{\mathbf{r}}_{ij} \quad (3.5)$$

where  $\theta_{ij}(t)$  is randomly fluctuating variable with Gaussian statistics:  $\langle\theta_{ij}(t)\rangle = 0$  and  $\langle\theta_{ij}(t)\theta_{kl}(t')\rangle = (\delta_{ik}\delta_{jl} + \delta_{il}\delta_{jk})\delta_{ij}(t-t')$ .

It has been proved that [Español and Warren, 1995] only one of the two weight functions in  $\mathbf{F}_{ij}^R$  and  $\mathbf{F}_{ij}^D$  can be defined arbitrarily and the other weight function is fixed accordingly.

In the DPD method, the individual atoms or molecules are not directly represented by particles, but they are grouped together into beads. These beads are free to move independently. Some molecules, such as polymers and surfactants must be represented by more than one bead. Therefore, an additional force between consecutive beads must be included to ensure chain connectivity:

$$\mathbf{F}_{i,i+1}^{\text{spring}} = K\mathbf{r}_{i,i+1} \quad (3.6)$$

The only parameter where the nature of the beads enters is the conservative force, because dissipation and noise are coupled. The relationship between Flory-Huggins interaction parameter  $\chi$  and the repulsion parameter  $a_{ij}$  acting between neighbouring beads is established by Groot and Warren [1997]. The repulsion parameter is proportional to the energy of mixing.  $\chi$  parameter can be calculated from solubility parameters or cohesive energy density values:

$$\chi_{AB} = \frac{V_{bead}}{kT} (\delta_A - \delta_B)^2 \quad (3.7)$$

where  $V_{bead}$  is the average molar volume of the beads,  $\delta_A$  and  $\delta_B$  are the solubility parameters of beads  $A$  and  $B$ , respectively. The value of solubility parameters depend on the chemical nature of the species in question.

### 3.1.2. MesoDyn

MesoDyn is based on the dynamic variant of the mean-field density functional theory, which indicates that there is a direct relationship between the distribution functions of the system, the densities, and an external potential field. The theory is similar to the classical dynamic random phase approximation (RPA) [de Gennes, 1979; Doi and Edwards, 1986]. The polymer chains are the fundamental building blocks of the method in MesoDyn and are modeled as ideal Gaussian chains consisting of beads. Each bead represents a number of monomers of the real polymer. The number of monomers in a bead is defined by the characteristic ratio of the polymer (i.e., they are Kuhn statistical segments).

The molecular ensemble is represented by a number,  $n$ , of Gaussian chains, made up of a number of different beads of types,  $I$ , with a total number  $N$  beads per chain. Throughout the simulation, at an instant of time there will be a certain distribution of bead positions in space that results in three-dimensional concentration fields,  $P(r)$ . The derivation of the diffusive dynamics of the molecular ensemble is

based on the assumption that for each type of bead,  $I$ , the local flux,  $\mathbf{J}_I$ , is proportional to the local bead concentration and the local thermodynamic driving force:

$$\mathbf{J}_I = -M\rho_I\nabla\mu_I + \tilde{\mathbf{J}}_I \quad (3.8)$$

where  $\tilde{\mathbf{J}}_I$  is a stochastic flux which can be thought of as thermal noise.  $M$  is the bead mobility parameter, analogous to self-diffusion coefficients. Combining this with the continuity equation:

$$\frac{\partial\rho_I}{\partial t} + \nabla \cdot \mathbf{J}_I = 0 \quad (3.9)$$

one gets simple diagonal functional Langevin equations in terms of density fields:

$$\frac{\partial\rho_I}{\partial t} = M\nabla \cdot \rho_I\nabla\mu_I + \eta_I \quad (3.10)$$

A Gaussian distribution of the noise is used.

However, the fluctuations in the total density of this simple system are not realistic, since finite compressibility is not enforced by the mean-field potential chosen. Therefore, total density fluctuations are simply removed by introducing the incompressibility constant:

$$(\rho_A(\mathbf{r},t))(\rho_B(\mathbf{r},t)) = \frac{1}{\nu_B} \quad (3.11)$$

where  $\nu_B$  is the average bead volume. This condition then leads to “exchange” Langevin equations:

$$\frac{\partial\rho_A}{\partial t} = M\nu_B\nabla \cdot \rho_A\rho_B\nabla[\mu_A - \mu_B] + \eta \quad (3.12)$$

and

$$\frac{\partial \rho_B}{\partial t} = M \nu_B \nabla \cdot \rho_A \rho_B \nabla [\mu_B - \mu_A] + \eta \quad (3.13)$$

The kinetic coefficient ( $M \nu_B \rho_A \rho_B$ ) models a local exchange mechanism. Hence the model is strictly valid only for Rouse dynamics [de Gennes, 1991]. Effects such as reptation lead to kinetic coefficients which extend over a range of roughly the coil size. They lead to computationally expensive nonlocal operators which in addition, are very complex in the non-linear regime.

The distribution of the Gaussian noise satisfies the fluctuation-dissipation theorem:

$$\langle \eta(\mathbf{r}, t) \rangle = 0 \quad (3.14)$$

and

$$\langle \eta(\mathbf{r}, t) \rangle \langle \eta(\mathbf{r}', t') \rangle = -\frac{2M \nu_B}{\beta} \delta(t - t') \nabla_{\mathbf{r}} \cdot \delta(\mathbf{r} - \mathbf{r}') \rho_A \rho_B \nabla_{\mathbf{r}} \quad (3.15)$$

which ensures that the time-integration of the Langevin equations generates an ensemble of density fields with Boltzmann distributions.

The non-ideal interactions between the chains are introduced by a mean field potential with the following form:

$$F^{\text{nid}}[\rho] = \frac{1}{2} \sum_{IJ} \iint \varepsilon_{IJ}(\mathbf{r} - \mathbf{r}') \rho_I(\mathbf{r}) \rho_J(\mathbf{r}') d\mathbf{r} d\mathbf{r}' \quad (3.16)$$

where  $\rho_I(\mathbf{r})$  is the density of bead type  $I$  at  $\mathbf{r}$  (local bead concentration), and  $\varepsilon_{IJ}(\mathbf{r}-\mathbf{r}')$  is a cohesive interaction between beads  $I$  at  $\mathbf{r}$  and  $J$  at  $\mathbf{r}'$ . Cohesive interaction is chosen to have a Gaussian form:

$$\varepsilon_{IJ}(|\mathbf{r}-\mathbf{r}'|) = \varepsilon_{IJ}^0 \left( \frac{3}{2\pi\alpha^2} \right)^{3/2} e^{-3/2\alpha^2(|\mathbf{r}-\mathbf{r}'|)^2} \quad (3.17)$$

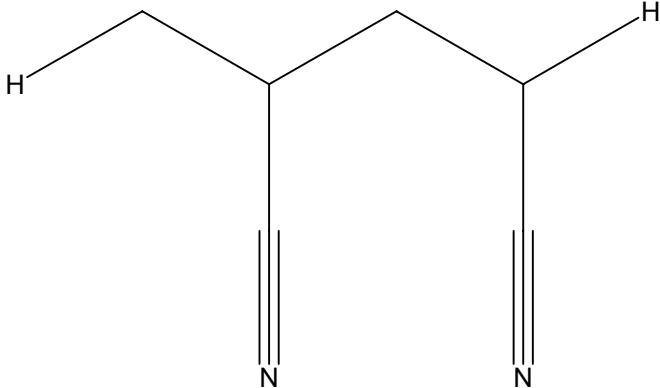
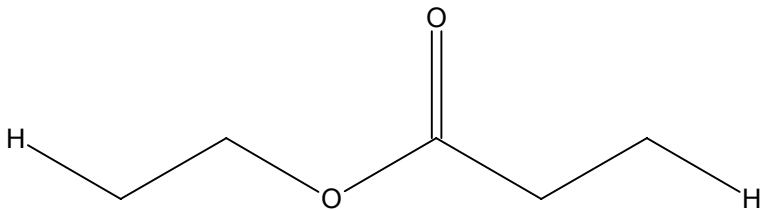
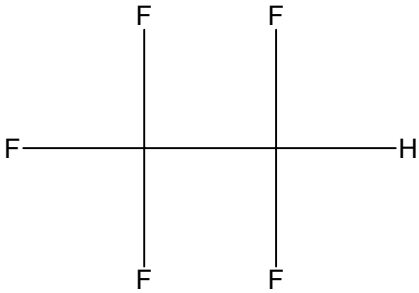
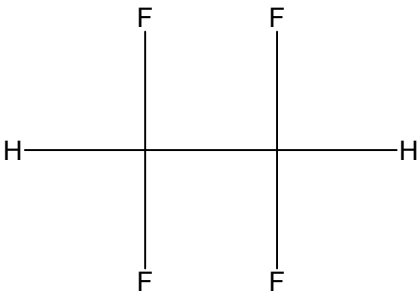
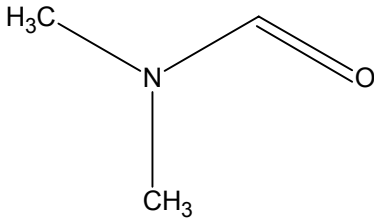
where  $\alpha$  is the Gaussian bond length and  $\varepsilon_{IJ}^0$  is the constant cohesive interaction between beads  $I$  and  $J$  which can be taken to be equal to the Flory-Huggins  $\chi$  parameter.

## 3.2. Results and Discussion

### 3.2.1. Interaction Energy and Parameterization

To construct systems for the DPD and MesoDyn methods, both polymer chains used in this study are divided into four bead types. Also, each DMF molecule is taken as one bead (Table 3.1). Since, the fluorine containing segments have different chemical properties from the ester and the acrylonitrile containing segments, they are constructed as separate beads. Two extra hydrogen atoms are attached to the connection points in all beads, excluding the solvent, to obtain consistency.

In DPD and MesoDyn methods, the interaction parameters are dependent on the  $\chi$  parameter that can be calculated from the solubility parameters. Therefore, atomistic simulations are made on the beads and results are supplied to coarse-grained simulations.  $\chi$  interaction parameter between two beads can be calculated from equation 3.7.

Bead Name	Structure
<p><b>C</b> (MW= 108.1 g/mol)</p>	
<p><b>E</b> (MW= 102.1 g/mol)</p>	
<p><b>F</b> (MW= 120.0 g/mol)</p>	
<p><b>H</b> (MW= 102.0 g/mol)</p>	
<p><b>D (DMF)</b> (MW= 73.1 g/mol)</p>	

**Table 3.1.** Beads used in the DPD and MesoDyn simulations.

All beads are built as shown in Table 3.1 and for geometry optimization, smart minimization is performed for 20000 steps. Amorphous Cell module is used for further simulations. Simulation boxes of the same type of 10 beads with density 1.0 are constructed. Then the simulation boxes, at 298 K, are equilibrated for 1 ps and further 10 ps MD simulations are performed to estimate solubility parameters. Periodic boundary conditions with a cutoff radius of 8.5 Å for all nonbonded interactions are employed in the canonical ensemble ( $NVT$ ). Initial velocities are assigned from a Maxwell-Boltzmann distribution in such a way that the total momentum in all directions sum up to zero. COMPASS forcefield is used in geometry optimizations and MD simulations.

MD simulation results are used to calculate solubility parameters and cohesive energy densities. Molar volumes (Table 3.2) are calculated using ACDLabs/ChemSketch 5.0 software package [Advanced Chemistry Development Inc.].

Bead	Solubility Parameter ( $\text{J}/\text{cm}^3$ ) <sup>1/2</sup>	Molar Volume ( $\text{cm}^3/\text{mol}$ ) $\mp$ 3
F	9.69	89.2
H	13.52	84
C	25.44	114.7
E	20.35	114.5
D	25.14	82.6

**Table 3.2.** Solubility parameters and molar volumes of the beads.

Theoretically, liquids with similar cohesive energy densities should have similar solubility characteristics. The  $\chi$  parameters (Table 3.3) show that fluorine containing segments are immiscible with other segments including the solvent. The smaller solubility parameter of  $\text{CF}_3\text{CF}_2\text{-H}$  molecule compared to  $\text{H-CF}_2\text{CF}_2\text{-H}$  shows that the immiscibility of fluorine containing segments can be increased by increasing the

fluorine content of the structure. Other beads, on the other hand, have larger solubility parameters due to their chemical structure. Solubility parameter is related to the molar energy of vaporization,  $\Delta E_v$  :

$$\delta = \left( \frac{\Delta E_v}{V_m} \right)^{1/2} = (CED)^{1/2} \quad (3.18)$$

where  $V_m$  is molar volume and  $CED$  is the cohesive energy density.

It is obvious that the molar energy of vaporization for the nonpolar materials should be smaller due to their weak intermolecular energies. The polar parts give rise to the cohesive energy density, and this is what is calculated in this study for the ester and acrylonitrile containing groups.

MesoDyn and DPD interaction parameters are calculated using  $\chi$  parameter. For the DPD method, Groot derived a relationship between  $\chi_{ij}$  parameter and repulsion parameter  $a_{ij}$  [Groot et al., 1997] between bead  $i$  and  $j$ . This relationship changes with the density and in our calculations we set the density at 3.

$$a_{ij} = \frac{\chi_{ij}}{0.306} + 25 \quad (3.19)$$

MesoDyn interaction parameter is given by:

$$v^{-1} \varepsilon_{ij} = \chi_{ij} RT \quad (3.20)$$

These are tabulated in Table 3.3.

$\chi_{ij}$	F	H	C	E	D
F	0.0000				
H	0.5110	0.0000			
C	10.1500	5.6641	0.0000		
E	4.6420	1.8544	1.1934	0.0000	
D	8.2283	4.5135	0.0031	0.9088	

$a_{ij}$ (DPD)	F	H	C	E	D
F	25.00				
H	26.67	25.00			
C	58.17	43.51	25.00		
E	40.17	31.06	28.9	25.00	
D	51.89	39.75	25.01	27.97	25.00

$v^{-1}\epsilon_{ij}$ (kJ/mol)	F	H	C	E	D
F	0				
H	1.25	0			
C	24.88	13.88	0		
E	11.38	4.55	2.93	0	
D	20.17	11.06	0	2.23	0

**Table 3.3.**  $\chi$ , conservative repulsion, and  $\chi$ -like MesoDyn parameters.

Attaching -H atoms for the consistency of the beads may lead to small differences in the calculation of solubility parameters. In our study these differences are ignored.

## 3.2.2. Mesoscale Calculations of the Fluorinated Polymers

### 3.2.2.1. DPD simulations

Polymer chain architecture is constructed as F-H<sub>2</sub>-E-C<sub>10</sub>-E-H<sub>2</sub>-F and C<sub>2</sub>E(H<sub>2</sub>F)[C<sub>5</sub>E(H<sub>2</sub>F)]<sub>4</sub>C<sub>3</sub>E(H<sub>2</sub>F) for the linear and graft polymer chains, respectively (Figure 3.1). DPD cubic boxes of size  $10 \times 10 \times 10 r_c^3$  are constructed with a density of 3 DPD units where  $r_c$  is the cutoff radius. The spring constant is chosen as 4.0 for the polymer chain beads [Groot et al., 1997]. Simulation temperature and bead masses are set to unity for simplicity. The total number of beads including polymer chains and solvents are set to 3000 in vacuum. Different concentrations of the polymer (20%, 30%, and 40%) are equilibrated for 20000 DPD steps followed by 80,000 steps of data collection.

Molecules are in constant motion, rotating and moving about in erratic ways, so the notion of structure has meaning only in an average sense. There are many possible ways to quantify this average structure. The radial distribution function (RDF) is one such way. The RDF addresses the question, "given an atom at some position, how many atoms can be expected at a distance  $r$  away from it?" More precisely, one seeks the number of atoms at a distance between  $r$  to  $r + dr$ . In our study, the results of the DPD simulations have similar radial distribution functions (Figure 3.2) indicating that the inter-bead interactions are softly repulsive. This result is contrary to classical methods such as MD and Brownian Dynamics (BD) where interactions are strongly repulsive at very short distances and weakly attractive at and beyond the atomic length scale. This property of DPD allows simulating the systems with larger time and length scales.

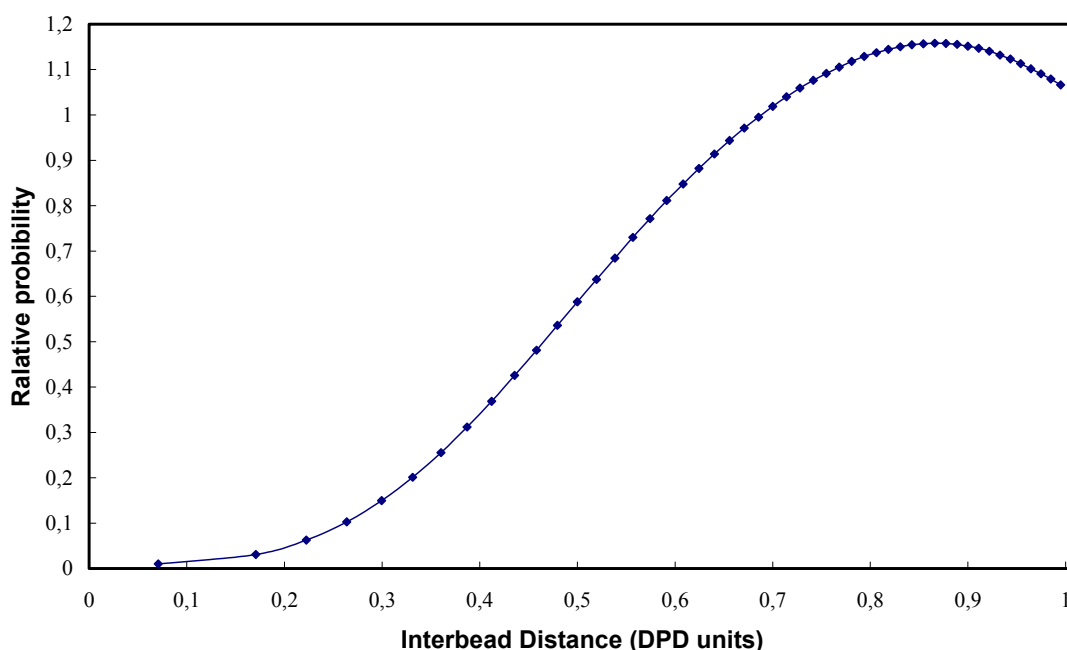


**Figure 3.2.** Radial distribution function

Prediction of polymer-solvent phase separation is very important to synthesize polymers for novel applications, because most of the time, removal of solvent after the polymerization process is very difficult. Mesoscale morphologies of graft and linear fluorinated polymers in DMF and in vacuum can be predicted by DPD simulations. It has been shown that polymers in solvent have spherical morphologies (Figure 3.3 and Figure 3.4). Since solubility parameters of the fluorine containing segments are small, these segments tend to move away from solvent molecules. Yet, just as in the MD simulations of Chapter 2, the chemical connectivity of fluorine containing segments with other solvophilic parts of the polymer does not allow the polymer to spread out. On the other hand, the DPD simulation of the linear polymer is lamellae and the self-assembly of the system occurs in the first 2000 time steps.

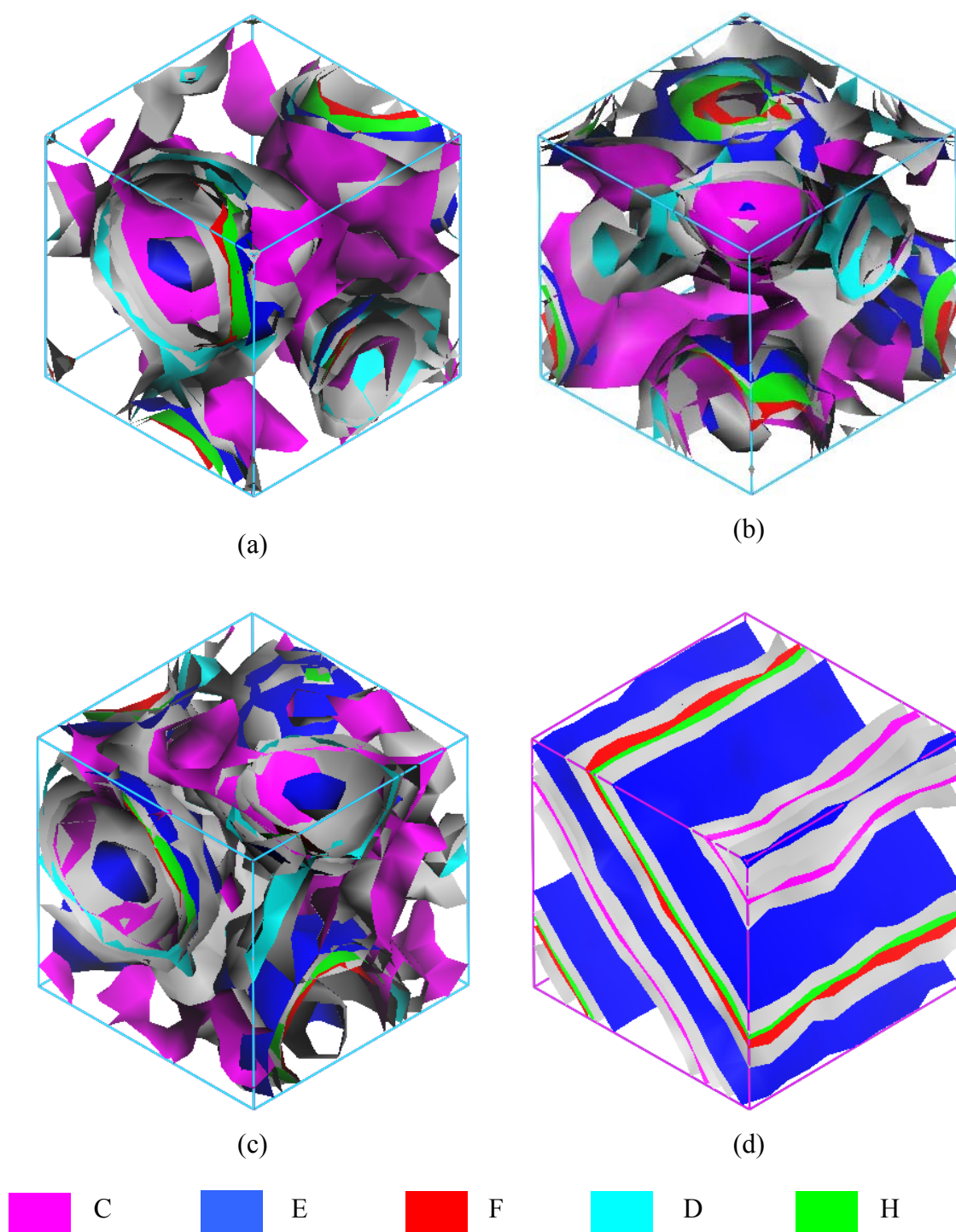


**Figure 3.3.** Isosurface morphologies of linear fluorinated polymers at different concentrations (a) 20% in DMF (b) 30% in DMF (c) 40% in DMF (d) pure polymer.

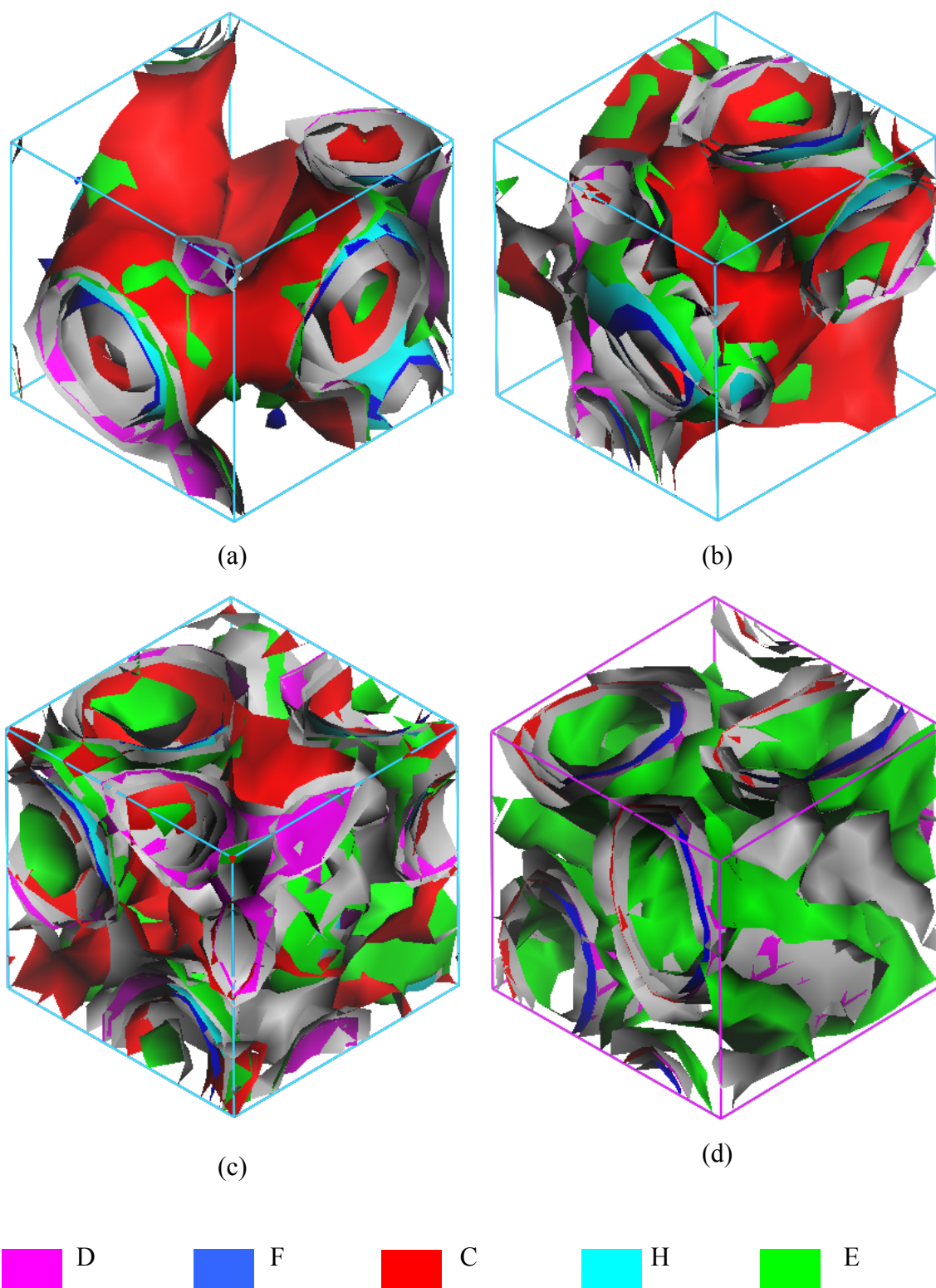


**Figure 3.4.** Isosurface morphologies of graft fluorinated polymers at different concentrations (a) 20% in DMF (b) 30% in DMF (c) 40% in DMF (d) pure polymer

Root mean square (RMS) end-to-end distances for the polymer chains are calculated in DPD units. Linear polymer consists of 18 beads and the graft polymer has 30 beads in its parent chain. Therefore, the polymers are long enough to sample different conformations in the solvent. RMS values can give us information on how the conformations of individual chains differ with changing concentration (Figure 3.5).

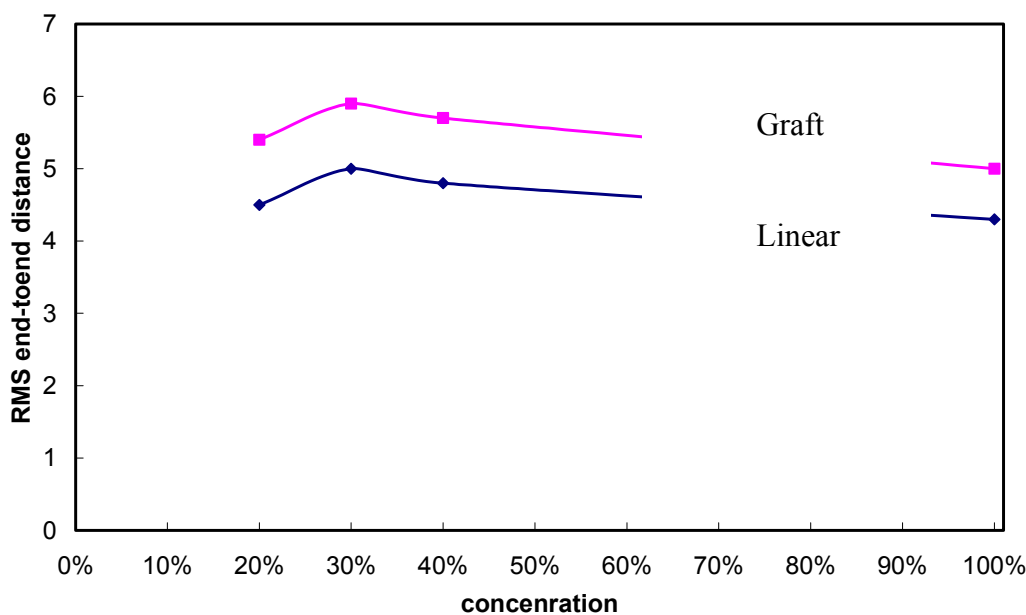


**Figure 3.5.** RMS end-to-end distances of linear and graft fluorinated polymers.

RMS end-to-end distance does not change by a significant amount by changing the composition of the polymer-solvent system. Pure chain simulations also show similar results. The characteristic size of individual chains in the system are the same in each environment, but their relative positioning in the bulk of the system changes so that different morphologies are obtained. Since DPD is a coarse-grained method and the only parameter that carries the atomistic information is the  $\chi$  parameter, these results should be verified using other conformational search methods (e.g. high temperature Molecular Dynamics).

One of the useful properties of DPD is that it can predict the interfacial tensions of complex fluids. In the literature, ternary phase diagram of oil-water-surfactant system is predicted by using DPD method and results were in excellent agreement with the experimental phase diagram [Yuan et al., 2002]. The interfacial tension between binary

interfaces can be calculated in the z-direction in the simulated cell using the following expression:

$$\sigma = \int \left\{ p_{zz}(z) - \frac{1}{2} [p_{xx}(x) + p_{yy}(y)] \right\} \quad (3.21)$$

where  $p_{ii}$  ( $i = x, y, z$ ) is the pressure in the  $i$  direction. In our study, interfacial tension results are calculated from the simulated systems (Table 3.4) and results for the polymer-solvent systems are close to each other. It is evident that the phase behaviours are similar in the solvent. On the other hand, interfacial tensions of pure linear and graft systems polymer are 0.280 and 0.860, respectively. This difference is due to the phase behaviours: LFP is lamellae and GFP is spherical.

Acatay et al. found that the contact angles of water with the graft fluorinated polymers are larger than those linear polymers [Acatay et al., 2004]. According to Young's equation, contact angle increases with the increased interfacial tension:

$$\gamma_2 \cos \theta = \gamma_1 - \gamma_{12} \quad (3.22)$$

where  $\gamma_1$  and  $\gamma_2$  are surface tensions of the components,  $\gamma_{12}$  and  $\theta$  are the interfacial tension and contact angle between the components, respectively. This equation indicates that the contact angle should increase with the interfacial tension. Our simulation results verify that the contact angles of the graft fluorinated polymers are bigger than the linear polymers.

Interfacial tensions	20%	30%	40%	pure
Linear Polymer	0.053	0.066	0.070	0.280
Graft Polymer	0.101	0.089	0.071	0.860

**Table 3.4.** Interfacial tensions at different concentrations.

### 3.2.2.2.MesoDyn Simulations

Two systems are simulated using MesoDyn method; pure linear polymer and 20% graft polymer.  $16 \times 16 \times 16 \text{ nm}^3$  MesoDyn boxes were constructed and equilibrated for 1000 steps. The MesoDyn simulations were subsequently continued for 10,000 steps. Langevin equations were integrated using Crank-Nicholson method.

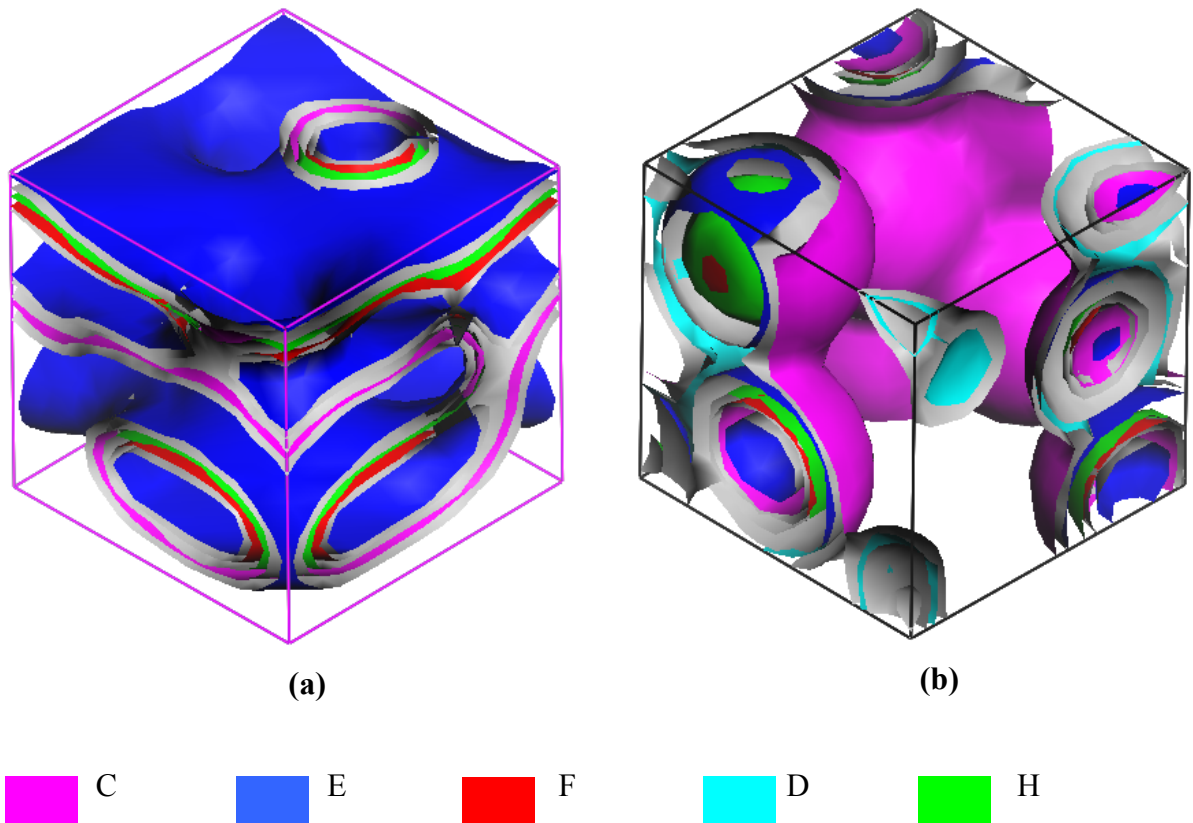


**Figure 3.6.** Isosurface representations of the (a) Pure linear polymer (b) 20% Graft polymer.

It is interesting to observe that the phase morphologies for these systems are similar to the DPD results. The pure linear polymer and 20% graft polymer form lamellae and spherical structures, respectively (Figure 3.6). Although the lamellar phase behaviour is a little bit destroyed, the mesoscale morphology of the linear polymer shows the same phase morphology as can be seen when comparing Figure 3.6a and

3.3d. In the 20% graft case (Figure 3.6b and 3.4a), spherical phases are nearly the same. Although DPD and MesoDyn use different approaches for the simulations of mesoscale structures, they can be used interchangeably to predict three-dimensional phase behaviour.

## CHAPTER 4

### CONCLUSIONS AND SUGGESTIONS FOR THE FUTURE WORK

Understanding the properties of fluorinated polymers is essential to improve their novel properties. In this thesis, computer simulations of linear and graft fluorinated polymers were made at the quantum level as well as the atomistic and mesoscopic scales.

The semiempirical quantum mechanical approach can not optimize the structure of the polymers to their global minima of the potential energy surface and is not an appropriate method for conformational search analysis of the long chain polymers. On the other hand, semiempirical approaches are useful for predicting the heats of formation, polarizabilities, and  $^{13}\text{C}$  chemical shifts, etc. The AM1 method is used and  $^{13}\text{C}$  chemical shifts are similar with the referenced carbon atoms, especially for  $-\text{CF}$  region.

The polarization of the linear fluorinated polymer increases with the applied external electric field and the density. The main structural unit causing the increase in polarization is the polar  $-\text{CN}$  groups. The total alignment of the  $-\text{CN}$  functional groups occurs only at electric fields on the order of  $1 \times 10^{11}$  eV/m, whereas only partial alignment occurs at lower fields. Since the apolar fluorine containing blocks are not affected by the external electric field, chain conformations are reorganized so as to indirectly increase the fluorine content of the system opposite to the direction of the electric field. If we consider the simulation box as a thin film, applying external electric field can increase fluorine content on the surface. This may be useful for the designation of fluorine-rich surfaces leading to low surface energy and high contact angles. Moreover, these results provide evidence as to the shift of surfaces from hydrophobic in

cast films (contact angle  $\sim 100^\circ$ ) to superhydrophobic in electrospun fibers (contact angle above  $140^\circ$ ) of the same polymeric chain.

The Flory-Huggins parameters show that fluorine containing segments are immiscible with other segments of the polymer chain and also with the solvent. Since fluorine containing segments are nonpolar or nearly nonpolar, the interparticle energies are small, leading to low solubility parameters. On the other hand, polar molecules have high solubility parameters due to their strong interparticle interactions (e.g. hydrogen bonding). Increasing the fluorine containing moieties in a molecule will decrease its solubility parameter, and thus  $\chi$  parameter between fluorine containing segments and polar segments will increase.

The results of the DPD simulations have similar radial distributions function indicating that the inter-bead interactions are softly repulsive. This result is contrary to classical methods such as MD and BD where interactions are strongly repulsive at very short distances and weakly attractive at and beyond the atomic length scale. This property of DPD allows simulating the systems with larger time and length scales.

Polymer-solvent interaction and phase separation is very important for the polymerization process. Most of the time, removal of the solvent is very difficult after completion of polymerization. Predicting the polymer-solvent phase behaviour can help experimentalists in designing synthesis procedures of polymers for novel applications. DPD simulations show that graft and linear fluorinated polymers form spherical micelles in an aprotic solvent. Pure linear polymer, on the other hand, is lamellae shaped. Two systems are constructed to compare DPD and MesoDyn methods and corresponding systems have similar morphologies. Although DPD and MesoDyn use different approaches for the simulations of mesoscale structures, they can be used interchangeably to predict three-dimensional phase behaviour. RMS values resulting from DPD simulations show that changing the concentration of the polymer in the solvent does not change the size of individual chains significantly. However, the relative positioning of the chains in the bulk of the system changes so that different morphologies are obtained.

In future work, systems that are obtained from MD simulations under external electric field will be further utilized. Atomistic simulations will be performed at the interface between the fluorine-rich surface and water. Dynamic properties of water close to the surface and far away from the surface will be investigated. In this way one can determine the difference in the behaviour of water molecules near superhydrophobic surfaces. Recently, Kyrylyuk et al. [2003] have incorporated the effect of external electric field into their dynamic density functional methodology, and have obtained impressive results corroborating experimental findings on diblock copolymer microdomains [Zvelindovsky and Svelink, 2003]. Similarly, morphologies of the current fluorinated systems under strong external electric field will be analyzed using Mesodyn to gain deeper understanding of the observed experimental phenomena by Acatay et al. [2004].

## APPENDIX A

### CONSISTENT FORCE FIELD-COMPASS

COMPASS has the same functional form with other consistent forcefields (e.g. CFF91, CFF, and PCFF). These methods are mainly differing in the range of functional groups to which they were parameterized and having slightly different parameter values. The functional form used in this forcefield [Sun et al., 1998]:

$$\begin{aligned}
 E_{total} = & \sum_b \left[ k_2(b-b_0)^2 + k_3(b-b_0)^3 + k_4(b-b_0)^4 \right] + \\
 & \sum_\theta \left[ k_2(\theta-\theta_0)^2 + k_3(\theta-\theta_0)^3 + k_4(\theta-\theta_0)^4 \right] + \\
 & \sum_\phi \left[ k_1(1-\cos\phi) + k_2(1-\cos 2\phi) + k_3(1-\cos 3\phi) \right] + \\
 & \sum_\chi k_2 \chi^2 \sum_{b,b'} k(b-b_0)(b'-b'_0) + \sum_{b,\theta} k(b-b_0)(\theta-\theta_0) + \\
 & \sum_{b,\phi} (b-b_0) \left[ k_1 \cos\phi + k_2 \cos 2\phi + k_3 \cos 3\phi \right] + \\
 & \sum_{\theta,\phi} (\theta-\theta_0) \left[ k_1 \cos\phi + k_2 \cos 2\phi + k_3 \cos 3\phi \right] + \\
 & \sum_{\theta,\theta'} k(\theta-\theta_0)(\theta'-\theta'_0) + \sum_{\theta,\theta',\phi} k(\theta-\theta_0)(\theta'-\theta'_0) \cos\phi + \\
 & \sum_{i,j} \frac{q_i q_j}{r_{ij}} + \sum_{i,j} \epsilon_{ij} \left[ 2 \left( \frac{r_{ij}^0}{r_{ij}} \right)^9 - 3 \left( \frac{r_{ij}^0}{r_{ij}} \right)^6 \right]
 \end{aligned} \tag{A.1}$$

The function can be divided into two categories which are valence terms including diagonal and off-diagonal cross-coupling terms and nonbonded interaction terms. The

valence terms represent internal coordinates of bond ( $b$ ), angle ( $\theta$ ), torsion angle ( $\phi$ ), and out-of plane angle ( $\chi$ ), and the cross coupling terms include combinations of two or three internal coordinates. The nonbonded interactions, which include a LJ-9-6 [Lifson et al., 1979] function for the van der Waals term and a Coulombic function for an electrostatic interaction, are used for interactions between pairs of atoms that are separated by two or more intervening atoms or those that belong to different molecules.

COMPASS is a powerful forcefield supporting atomistic simulations of condensed phase materials. COMPASS stands for Condensed-phase Optimized Molecular Potentials for Atomistic Simulations Studies. This is the first *ab initio* forcefield that has been parameterized and validated using condensed-phase properties in addition to various *ab initio* and empirical data for molecules in isolation. Consequently, this forcefield enables accurate and simultaneous prediction of structural, conformational, vibrational, and thermophysical properties for a broad range of molecules in isolation and in condensed phases including common organic molecules, inorganic small molecules and polymers.

## BIBLIOGRAPHY

Acatay K., PhD Thesis, Sabanci University, Istanbul, Turkey, 2004.

Accelrys Inc., Materials Studio, San Diego: Accelrys Inc., 2002.

ACDLabs/ChemSketch, version 5.0, Advanced Chemistry Development, Inc., Toronto ON, Canada, www.acdlabs.com, 2003.

Albert, B.; Jerome, R.; Teyssié, P. *Macromol. Chem.*, **185**, 579, 1984.

Adler, B. J. and T. E. Wainwright, *J. Chem. Phys.* **27**, 1208, 1957.

Allen, M. P. and D. J. Tildesley, "Computer Simulation of Liquids", Clarendon Press, 1989.

Altevogt, P., O. A. Evers, J. G. E. M. Fraaije, N. M. Maurits, B. A. C. van Vlimmeren, "The MesoDyn Project: Software for Mesoscale Chemical Engineering", *J. Mol. Struct. (Theochem)*, **463**, 139, 1999.

Ameduri, B.; Boutevin, B.; Guida-Pietrasanta, F.; Rousseau *J. Fluorine Chem.*, **107**, 397, 2001.

Andersen, H. C., "Molecular Dynamics Simulations at Constant Pressure and/or Temperature", *J. Chem. Phys.*, **72**, 2384, 1980.

Batchelor, G. K. "An Introduction to Fluid Dynamics", Cambridge University Press, 1992.

Baysal, C. and H. Meirovitch, "Efficiency of Simulated Annealing for Peptides with Increasing Geometrical Restrictions", *J. Comput. Chem.*, **20**, 1659, 1999

Bilgin, N., C. Baysal, Y. Z. Menciloglu, *Polymer*, submitted, 2004.

Bird, R. B., R. C., Armstrong, and O. Hassager, *Dynamics of Polymeric Liquids*, Wiley, 1987.

Boghosian, B. M., F. J. Alexander and P. V. Coveney, "Proceedings of the 1996 Conference on Discrete Models for Fluid Mechanics", *Int. J. Mod. Phys. C*, **8**, 1997.

Bouteiller, V.; Garnault, A. M.; Teyssié, D.; Boileau, S.; Möller, M. *Polym. Int.*, **48**, 1999

Chaudhury, M. K.; Whitesides, G. M. *Science*, **255**, 1230, 1992

Clark, T. G. Rauhut and A. Breindl, *J. Mol. Mod.*, **1**, 22, 1995.

Clark, T., A. Alex, B. Beck, F. Burkhardt, J. Chandrasekhar, P. Gedeck, A. Horn, M. Hutter, B. Martin, G. Rauhut, W. Sauer, T. Schindler, T. Steinke, *VAMP*, version 8.1, Universität Erlangen, Erlangen, Germany, 2002. This version is provided as part of Materials Studio 2.2. by Accelrys Inc.

Cohen, E. G. D., "Fundamental Problems in Statistical Mechanics", **1**, 110 North Holland Publishing Company, Amsterdam, 1962.

DeSimone, J. M., Guan, Z., Elsbernd, C. S. *Science*, **257**, 945, 1992.

Dewar, M. J. S., and W. Thiel, "Ground States of Molecules, 38, The MNDO Approximations and Parameters", *J. Am. Chem. Soc.*, **99**, 22, 4899, 1977.

Dewar, M. J. S., E. G. Zoebisch, E. F. Healy and J. J. P. Stewart, "AM1: A New General Purpose Quantum Mechanical Molecular Model", *J. Am. Chem. Soc.*, **107**, 3902, 1985.

Doi, M., S. F. Edwards, *The Theory of Polymer Dynamics*, Clarendon, Oxford, England, 1986.

Doolen, G. D., *Lattice Gas Methods for Partial Differential Equations*, Addison-Wesley Publishing Company, 1990.

Espanol, P. and P. B. Warren, "Statistical Mechanics of Dissipative Particle Dynamics", *Europhys. Lett.*, **30**, 191, 1995

Ferrante, A., "Fundamentals of the Dynamics in Concentrated Suspensions", *Curr. Opinion in Colloid and Interface Sci.*, **1**(6), 820, 1996.

Fletcher, R., "Unconstrained Optimization", *Practical Methods of Optimization*, **1**, John Wiley&Sons, New York, 1980.

Fraaije, J. G. E. M., B. A. C. van Vlimmeren, N. M. Maurits, M. Postma, O. A. Evers, C. Hoffman, P. Altevogt and G. Goldbeck, "The Dynamic Mean-field Density Functional method and Its Application to the Mesoscopic Dynamics of Quenched Block Copolymer Melts", *J. Chem. Phys.*, **106**, 4260, 1997.

Frisch, U., B. Hasslacher and Y. Pomeau, "Lattice-gas Automata for the Navier-Stokes Equations", *Phys. Rev. Lett.*, **56**, 1505, 1986.

de Gennes, P. G., *Scaling Concepts in Polymer Physics*, Cornell University, Ithaca, NY, 1991.

Groot, R. D. and P. Warren, "Dissipative Particle Dynamics: Bridging the Gap Between Atomistic and Mesoscopic Simulation", *J. Chem. Phys.*, **107**, 191, 1997.

Guyot, B.; Ameduri, B.; Boutevin, B. *J. Fluorine Chem.*, **74**, 233, 1995.

Hoogerbrugge, P. J. and J. M. V. A. Koelman, "Simulating Microscopic Hydrodynamics Phenomena with Dissipative particle Dynamics", *Europhys. Lett.*, **19**, 155, 1992.

Höpken, J.; Möller, M. *Macromolecules*, **25**, 2482, 1992.

Hwang, S. S.; Ober, C. K.; Perutz, S. M.; Iyengar, D. R.; Schneggenburger, L. A.; Kramer, E. J. *Polymer*, **36**, 1321, 1995

Johnson, R. E. Jr., Dettre, R. H. in *Wettability*; Berg, J. C., Ed.; Marcel Dekker: New York, Chapter 1, 1993.

Jones, R. A. L., Richards, R. W. *Polymers at Surfaces and Interfaces*, Cambridge University Press, Cambridge, 1999, and references therein.

Kato, S., Ueno, Y., Kishida, A., Miyazaki, T., Matsumoto, T., Murata, Y., Akashi, M. *J. Appl. Polym. Sci.* **71**, 1049, 1999

Kobayashi, H.; Owen, M. J. *Trends Polym. Sci.*, **3**, 10, 1995

Kyrylyuk A. V., G. J. A. Sevink, A. V. Zvelindovsky, J. G. E. M. Fraaije, "Simulations of electric field induced lamellar alignment in block copolymers in the presence of selective electrodes", *Macromolecular Theory and Simulations*, **12**, 508, 2003.

Lambert, J. B., Shurvell, F. S., Lightner, D., Cooks, R. G., "Introduction to Organic Spectroscopy", Cellier Macmillan Publishers, London, 1997.

Marder, M. P., "Condensed Matter Physics", New York, John Wiley, 2000.

Maurits, N. M., A. V. Zvelindovsky, G. J. A. Sevink, B. A. C. van Vlimmeren, J. G. E. M. Fraaije, "Hydrodynamic Effects in 3D Microphase Separation of Block Copolymers: Dynamic Mean-field Density Functional Approach", *J. Chem. Phys.*, **108**, 500, 1998.

Mazzone, A. M., "Analysis of Serial and Parallel Algorithms for Use in Molecular Dynamics. Review and Proposals", *Int. J. Mod. Phys. C*, **9**(1), 179, 1998.

McLeish, T., "Theoretical Challenges in the Dynamics of Complex Fluids", *NATO ASI Series*, Kluwer, Dordrecht, **339**, 1997.

Morita, M., Ogisu, H., Kubo, M. *J. Appl. Polym. Sci.*, **73**, 1741, 1999.

Park, I. J., Lee, S. B., C. K. Choi, *Polymer*, **38**, 2523, 1997

Perutz, S. M., Dai, C. A., Ober, C. K., Kramer, E. J. *Macromolecules*, **29**, 1229, 1996

Perutz, S., Wang, J., Kramer, E. J., Ober, C. K., Ellis, K. *Macromolecules*, **31**, 4272, 1998

Plunkett, R. J. *U. S. Pat.* US 2230654.

Pople, J. A. and G. A. Segal, "An Approximate self-consistent molecular orbital theory II. Calculations with complete neglect of differential overlap", *J. Chem. Phys.*, **43**, 136, 1965

Powell, M. J. D., "Restart Procedure for the Conjugate Gradient Method", *Mathematical Programming*, **12**, 241, 1977.

Rothman, D. H., and J. M. Keller, "Immiscible Cellular Automata Fluids" *J. Stat. Phys.*, **52**, 1119, 1988.

Rothman, D. H. and Z. Zaleski, "Lattice Gas Models of Phase Separation-Interfaces, Phase Transitions and Multiphase Flow", *Rev. Mod. Phys.*, **66**, 1417, 1994.

Stewart, J. J. P. "Optimization of Parameters for Semiempirical Methods I. Method", *J. Comp. Chem.*, **10**, 209, 1989.

Sun, H., “COMPASS: An Ab Initio Forcefield Optimized for Condensed-Phase Applications – Overview with Details on Alkane and Benzene Compounds”, *J. Phys. Chem. B.*, **102**, 7338, 1998.

Thorpe, A. A.; Young, S. A.; Nevell, T. G.; Tsibouklis, J. *J. Appl. Surf. Sci.*, **136**, 99, 1998.

Verlet, L., “Computer Experiments on Classical Fluids: I. Thermodynamical Properties of Lennard-Jones Molecules”, *Phys. Rev.*, **159**, 98, 1967.

Yuan, S., Z. Cai, G. Xu, Y. Jiang, “Mesoscopic Simulation Study on Phase Diagram of the System Oil/Water/Aerosol OT”, *Chem Phys. Lett.*, **365**, 347, 2002.

Wang, J.; Mao, G.; Ober, C. K.; Kramer, E. J. *Macromolecules*, **30**, 1906, 1997.

Zisman, W. A. *Contact Angle, Wettability, and Adhesion*, Advances in Chemistry Series 43, Am. Chem. Soc.: Washington DC, 1964.

Zvelindovsky, A. V., G. J. A. Sevink, B. A. C. van Vlimmeren, N. M. Maurits, J. G. E. M. Fraaije, “3D Mesoscale Dynamics of Block Copolymers Under Shear: The Dynamic Density Functional Approach”, *Phys. Rev. E.*, **57**, 4699, 1998.

Zvelindovsky, A. V., G. J. A. Sevink, “Comment on Microscopic Mechanisms of Electric-Field-Induced Alignment of Block Copolymer Microdomains”, *Phys. Rev. Lett.*, **90**, 49601, 2003.

## BIBLIOGRAPHY

Acatay K., PhD Thesis, Sabanci University, Istanbul, Turkey, 2004.

Accelrys Inc., Materials Studio, San Diego: Accelrys Inc., 2002.

ACDLabs/ChemSketch, version 5.0, Advanced Chemistry Development, Inc., Toronto ON, Canada, www.acdlabs.com, 2003.

Albert, B.; Jerome, R.; Teyssié, P. *Macromol. Chem.*, **185**, 579, 1984.

Adler, B. J. and T. E. Wainwright, *J. Chem. Phys.* **27**, 1208, 1957.

Allen, M. P. and D. J. Tildesley, "Computer Simulation of Liquids", Clarendon Press, 1989.

Altevogt, P., O. A. Evers, J. G. E. M. Fraaije, N. M. Maurits, B. A. C. van Vlimmeren, "The MesoDyn Project: Software for Mesoscale Chemical Engineering", *J. Mol. Struct. (Theochem)*, **463**, 139, 1999.

Ameduri, B.; Boutevin, B.; Guida-Pietrasanta, F.; Rousseau *J. Fluorine Chem.*, **107**, 397, 2001.

Andersen, H. C., "Molecular Dynamics Simulations at Constant Pressure and/or Temperature", *J. Chem. Phys.*, **72**, 2384, 1980.

Batchelor, G. K. "An Introduction to Fluid Dynamics", Cambridge University Press, 1992.

Baysal, C. and H. Meirovitch, "Efficiency of Simulated Annealing for Peptides with Increasing Geometrical Restrictions", *J. Comput. Chem.*, **20**, 1659, 1999

Bilgin, N., C. Baysal, Y. Z. Menciloglu, *Polymer*, submitted, 2004.

Bird, R. B., R. C., Armstrong, and O. Hassager, *Dynamics of Polymeric Liquids*, Wiley, 1987.

Boghosian, B. M., F. J. Alexander and P. V. Coveney, "Proceedings of the 1996 Conference on Discrete Models for Fluid Mechanics", *Int. J. Mod. Phys. C*, **8**, 1997.

Bouteiller, V.; Garnault, A. M.; Teyssié, D.; Boileau, S.; Möller, M. *Polym. Int.*, **48**, 1999

Chaudhury, M. K.; Whitesides, G. M. *Science*, **255**, 1230, 1992

Clark, T. G. Rauhut and A. Breindl, *J. Mol. Mod.*, **1**, 22, 1995.

Clark, T., A. Alex, B. Beck, F. Burkhardt, J. Chandrasekhar, P. Gedeck, A. Horn, M. Hutter, B. Martin, G. Rauhut, W. Sauer, T. Schindler, T. Steinke, *VAMP*, version 8.1, Universität Erlangen, Erlangen, Germany, 2002. This version is provided as part of Materials Studio 2.2. by Accelrys Inc.

Cohen, E. G. D., "Fundamental Problems in Statistical Mechanics", **1**, 110 North Holland Publishing Company, Amsterdam, 1962.

DeSimone, J. M., Guan, Z., Elsbernd, C. S. *Science*, **257**, 945, 1992.

Dewar, M. J. S., and W. Thiel, "Ground States of Molecules, 38, The MNDO Approximations and Parameters", *J. Am. Chem. Soc.*, **99**, 22, 4899, 1977.

Dewar, M. J. S., E. G. Zoebisch, E. F. Healy and J. J. P. Stewart, "AM1: A New General Purpose Quantum Mechanical Molecular Model", *J. Am. Chem. Soc.*, **107**, 3902, 1985.

Doi, M., S. F. Edwards, *The Theory of Polymer Dynamics*, Clarendon, Oxford, England, 1986.

Doolen, G. D., *Lattice Gas Methods for Partial Differential Equations*, Addison-Wesley Publishing Company, 1990.

Espanol, P. and P. B. Warren, "Statistical Mechanics of Dissipative Particle Dynamics", *Europhys. Lett.*, **30**, 191, 1995

Ferrante, A., "Fundamentals of the Dynamics in Concentrated Suspensions", *Curr. Opinion in Colloid and Interface Sci.*, **1**(6), 820, 1996.

Fletcher, R., "Unconstrained Optimization", *Practical Methods of Optimization*, **1**, John Wiley&Sons, New York, 1980.

Fraaije, J. G. E. M., B. A. C. van Vlimmeren, N. M. Maurits, M. Postma, O. A. Evers, C. Hoffman, P. Altevogt and G. Goldbeck, "The Dynamic Mean-field Density Functional method and Its Application to the Mesoscopic Dynamics of Quenched Block Copolymer Melts", *J. Chem. Phys.*, **106**, 4260, 1997.

Frisch, U., B. Hasslacher and Y. Pomeau, "Lattice-gas Automata for the Navier-Stokes Equations", *Phys. Rev. Lett.*, **56**, 1505, 1986.

de Gennes, P. G., *Scaling Concepts in Polymer Physics*, Cornell University, Ithaca, NY, 1991.

Groot, R. D. and P. Warren, "Dissipative Particle Dynamics: Bridging the Gap Between Atomistic and Mesoscopic Simulation", *J. Chem. Phys.*, **107**, 191, 1997.

Guyot, B.; Ameduri, B.; Boutevin, B. *J. Fluorine Chem.*, **74**, 233, 1995.

Hoogerbrugge, P. J. and J. M. V. A. Koelman, "Simulating Microscopic Hydrodynamics Phenomena with Dissipative particle Dynamics", *Europhys. Lett.*, **19**, 155, 1992.

Höpken, J.; Möller, M. *Macromolecules*, **25**, 2482, 1992.

Hwang, S. S.; Ober, C. K.; Perutz, S. M.; Iyengar, D. R.; Schneggenburger, L. A.; Kramer, E. J. *Polymer*, **36**, 1321, 1995

Johnson, R. E. Jr., Dettre, R. H. in *Wettability*; Berg, J. C., Ed.; Marcel Dekker: New York, Chapter 1, 1993.

Jones, R. A. L., Richards, R. W. *Polymers at Surfaces and Interfaces*, Cambridge University Press, Cambridge, 1999, and references therein.

Kato, S., Ueno, Y., Kishida, A., Miyazaki, T., Matsumoto, T., Murata, Y., Akashi, M. *J. Appl. Polym. Sci.* **71**, 1049, 1999

Kobayashi, H.; Owen, M. J. *Trends Polym. Sci.*, **3**, 10, 1995

Kyrylyuk A. V., G. J. A. Sevink, A. V. Zvelindovsky, J. G. E. M. Fraaije, "Simulations of electric field induced lamellar alignment in block copolymers in the presence of selective electrodes", *Macromolecular Theory and Simulations*, **12**, 508, 2003.

Lambert, J. B., Shurvell, F. S., Lightner, D., Cooks, R. G., "Introduction to Organic Spectroscopy", Cellier Macmillan Publishers, London, 1997.

Marder, M. P., "Condensed Matter Physics", New York, John Wiley, 2000.

Maurits, N. M., A. V. Zvelindovsky, G. J. A. Sevink, B. A. C. van Vlimmeren, J. G. E. M. Fraaije, "Hydrodynamic Effects in 3D Microphase Separation of Block Copolymers: Dynamic Mean-field Density Functional Approach", *J. Chem. Phys.*, **108**, 500, 1998.

Mazzone, A. M., "Analysis of Serial and Parallel Algorithms for Use in Molecular Dynamics. Review and Proposals", *Int. J. Mod. Phys. C*, **9**(1), 179, 1998.

McLeish, T., "Theoretical Challenges in the Dynamics of Complex Fluids", *NATO ASI Series*, Kluwer, Dordrecht, **339**, 1997.

Morita, M., Ogisu, H., Kubo, M. *J. Appl. Polym. Sci.*, **73**, 1741, 1999.

Park, I. J., Lee, S. B., C. K. Choi, *Polymer*, **38**, 2523, 1997

Perutz, S. M., Dai, C. A., Ober, C. K., Kramer, E. J. *Macromolecules*, **29**, 1229, 1996

Perutz, S., Wang, J., Kramer, E. J., Ober, C. K., Ellis, K. *Macromolecules*, **31**, 4272, 1998

Plunkett, R. J. *U. S. Pat.* US 2230654.

Pople, J. A. and G. A. Segal, "An Approximate self-consistent molecular orbital theory II. Calculations with complete neglect of differential overlap", *J. Chem. Phys.*, **43**, 136, 1965

Powell, M. J. D., "Restart Procedure for the Conjugate Gradient Method", *Mathematical Programming*, **12**, 241, 1977.

Rothman, D. H., and J. M. Keller, "Immiscible Cellular Automata Fluids" *J. Stat. Phys.*, **52**, 1119, 1988.

Rothman, D. H. and Z. Zaleski, "Lattice Gas Models of Phase Separation-Interfaces, Phase Transitions and Multiphase Flow", *Rev. Mod. Phys.*, **66**, 1417, 1994.

Stewart, J. J. P. "Optimization of Parameters for Semiempirical Methods I. Method", *J. Comp. Chem.*, **10**, 209, 1989.

Sun, H., "COMPASS: An Ab Initio Forcefield Optimized for Condensed-Phase Applications – Overview with Details on Alkane and Benzene Compounds", *J. Phys. Chem. B.*, 102, 7338, 1998.

Thorpe, A. A.; Young, S. A.; Nevell, T. G.; Tsibouklis, J. *J. Appl. Surf. Sci.*, **136**, 99, 1998.

Verlet, L., "Computer Experiments on Classical Fluids: I. Thermodynamical Properties of Lennard-Jones Molecules", *Phys. Rev.*, **159**, 98, 1967.

Yuan, S., Z. Cai, G. Xu, Y. Jiang, "Mesoscopic Simulation Study on Phase Diagram of the System Oil/Water/Aerosol OT", *Chem Phys. Lett.*, **365**, 347, 2002.

Wang, J.; Mao, G.; Ober, C. K.; Kramer, E. J. *Macromolecules*, **30**, 1906, 1997.

Zisman, W. A. *Contact Angle, Wettability, and Adhesion*, Advances in Chemistry Series 43, Am. Chem. Soc.: Washington DC, 1964.

Zvelindovsky, A. V., G. J. A. Sevink, B. A. C. van Vlimmeren, N. M. Maurits, J. G. E. M. Fraaije, "3D Mesoscale Dynamics of Block Copolymers Under Shear: The Dynamic Density Functional Approach", *Phys. Rev. E.*, **57**, 4699, 1998.

Zvelindovsky, A. V., G. J. A. Sevink, "Comment on Microscopic Mechanisms of Electric-Field-Induced Alignment of Block Copolymer Microdomains", *Phys. Rev. Lett.*, **90**, 49601, 2003.